



LUND UNIVERSITY

Internal Dosimetry Development and Evaluation of Methods and Models

Jönsson, Lena M

2007

[Link to publication](#)

Citation for published version (APA):

Jönsson, L. M. (2007). *Internal Dosimetry Development and Evaluation of Methods and Models*. [Doctoral Thesis (compilation), Medical Radiation Physics, Lund]. Medical Radiation Physics, Lund University.

Total number of authors:

1

General rights

Unless other specific re-use rights are stated the following general rights apply:

Copyright and moral rights for the publications made accessible in the public portal are retained by the authors and/or other copyright owners and it is a condition of accessing publications that users recognise and abide by the legal requirements associated with these rights.

- Users may download and print one copy of any publication from the public portal for the purpose of private study or research.
- You may not further distribute the material or use it for any profit-making activity or commercial gain
- You may freely distribute the URL identifying the publication in the public portal

Read more about Creative commons licenses: <https://creativecommons.org/licenses/>

Take down policy

If you believe that this document breaches copyright please contact us providing details, and we will remove access to the work immediately and investigate your claim.

LUND UNIVERSITY

PO Box 117
221 00 Lund
+46 46-222 00 00

Internal Dosimetry

Development and Evaluation of Methods and Models

Lena Jönsson

Medical Radiation Physics
Department of Clinical Sciences, Lund
Lund University, Sweden
2007



LUND UNIVERSITY

Thesis for the Degree of Doctor of Philosophy
Faculty of Science at Lund University
Medical Radiation Physics
Department of Clinical Sciences, Lund
Lund University Hospital
SE-221 85 Lund, Sweden

Copyright 2007 Lena Jönsson (pp. 1-52)
ISBN 978-91-628-7090-4
Printed in Sweden by Media-Tryck, Lund, 2007

"Before I came here I was confused about this subject.
Having listened to your lecture I am still confused.
But on a higher level."

Enrico Fermi

Abstract

Radionuclide therapy requires patient-specific planning of the absorbed dose to target volumes, in most cases tumours, in order to achieve an expected biological effect, taking into account that the absorbed doses to normal organs and tissues should be kept as low as reasonably achievable. Therefore, the calculation of absorbed doses has to be as accurate as possible. The accuracy depends on the methods used for activity quantification and on how well the dosimetric model describes the organs and tissues in the particular patient.

This thesis presents new methodologies developed to investigate the accuracy of internal dosimetry. The main focus was on the use of detailed biokinetic data from animals combined with Monte Carlo simulations using anthropomorphic phantoms on macro level, and applied in the development and refinement of an intestinal dosimetry model on a small-scale level.

A novel approach is the generation of Monte Carlo simulated scintillation camera images of a computer patient using a radionuclide biodistribution obtained from an experimental animal study. The accuracy of the activity quantification based on planar scintillation camera imaging was investigated and in particular the corrections for attenuation and scatter with the presence of activity in overlapping tissues. The absorbed doses were calculated using phantom-specific dose factors (S values) and were compared with absorbed doses calculated from standard MIRD-phantom-based S values. The results demonstrate the potential inaccuracy of the calculated absorbed dose to an individual patient when using dose factors based on the MIRD phantom.

A dosimetry model for the small intestine was developed and refined in order to obtain a more accurate model and dose factors. Previous dosimetry models of the small intestine have been limited to calculating the absorbed dose to the intestinal wall from activity in the contents only. The work in this thesis included Monte Carlo calculations of dose factors for the radiation sensitive crypt cells as target organ. The activity in the contents as well as in the intestinal wall was taken into account, and dose factors were calculated for both self-dose and cross-dose from surrounding parts of the small intestine. Calculations of the absorbed dose to the crypt cells for a realistic activity distribution are presented and compared with results from the general absorbed dose calculation.

It is evident from the results in this thesis that improvements are necessary in the quantification procedure, as well as further development of more realistic, small-scale anatomy models.

Key words: Nuclear medicine, internal dosimetry, conjugate view method, Monte Carlo simulation, activity quantification, sestamibi, scintillation camera, radionuclide, intestine, crypt cells.

List of publications

This thesis is based of the following papers, which will be referred to by their roman numerals in the text.

- I Lena Jönsson, Xiaowei Liu, Bo-Anders Jönsson, Michael Ljungberg and Sven-Erik Strand.
A Dosimetry Model for the Small Intestine Incorporating Intestinal Wall Activity and Cross-Doses. *The Journal of Nuclear Medicine*, 43:1657-1664, 2002.
- II Lena Jönsson, Xiaowei Liu, Bo-Anders Jönsson, Michael Ljungberg and Sven-Erik Strand.
Crypt Cell Dosimetry for ^{99m}Tc -Sestamibi in a New Small Intestinal Dosimetry Model. *Cancer Biotherapy & Radiopharmaceuticals*, 18:217-223, 2003.
- III Lena Jönsson, Michael Ljungberg and Sven-Erik Strand.
Evaluation of Accuracy in Activity Calculations for the Conjugate View Method from Monte Carlo Simulated Scintillation Camera Images Using Experimental Data in an Anthropomorphic Phantom. *The Journal of Nuclear Medicine*, 46:1679-1686, 2005.
- IV Lena Jönsson, Michael Ljungberg and Sven-Erik Strand.
A Method to Evaluate the Accuracy of Internal Dosimetry. *The Journal of Nuclear Medicine* (Submitted).

Reprinting of the papers was kindly permitted by The Society of Nuclear Medicine (**Papers I and III**) and Mary Ann Liebert, Inc., publishers (**Paper II**).

Contents

Introduction	1
The Aim of the Present Investigation	3
The Basics of Internal Dosimetry	4
The Basics of the Monte Carlo Method	6
Principles	6
Photon Simulation	6
Charged-Particle Simulation	6
Public-Domain Programs	7
Phantoms	7
Activity Quantification	9
The Scintillation Camera.....	9
The Conjugate-View Attenuation Correction Method.....	11
Measurement of Attenuation Coefficients.....	13
Correction for Scatter.....	14
<i>The Effective Attenuation Coefficient</i>	15
<i>The Buildup Factor Method</i>	15
<i>The Triple-Energy Window Method</i>	17
Definition of Regions of Interest	19
Background Activity Correction	20
Activity in Overlapping Tissues.....	20
The Absorbed Dose Conversion Factor	23
General Geometrical Models of the Human Body	23
Scaling of Dose Conversion Factors	24
The Small Intestine as a Specific Case	27
<i>Previous Models</i>	28
<i>Our Extended Model</i>	29
Importance of an Improved Small Intestinal Model	31
Summary of Papers	33
Future Perspectives	36
Acknowledgements	40
References	41
Populärvetenskaplig sammanfattning	52

Introduction

In Sweden every year, more than 100 000 patients are scheduled for nuclear medicine diagnostic studies in which radiopharmaceuticals are administered (1). These patients normally receive only a small amount of activity, which results in a low absorbed dose to the organs, as well as a low effective dose. About 3000 of these patients are, however, given considerably higher activity for radionuclide therapy, leading to much higher absorbed doses. Developments in the field of radionuclide therapy have led to some new radiopharmaceuticals such as radiolabelled monoclonal antibodies specific to lymphoma B cells, e.g. ^{111}In - and ^{90}Y -labelled ibritumomab tiuxetan (Zevalin®, Schering Nordiska AB) and ^{131}I -tositumomab (Bexxar®, Corixa and GlaxoSmithKline Corporations) (2-5), accepted for clinical use. These are currently the only radiolabelled monoclonal antibodies approved for the treatment of cancer, of which ibritumomab tiuxetan is in use in Sweden. Future developments will probably lead to other radiopharmaceuticals for radionuclide therapy.

For the radiopharmaceuticals used in diagnostic nuclear medicine absorbed doses are estimated for radiation protection purposes with a method using a “standard” patient geometry (the MIRD phantom) (6). Dosimetry calculations involving patient-specific geometries are in general not performed. To make absorbed dose calculations as accurate as possible, the activity distribution must be measured at multiple points in time for a group of patients to generate time-activity curves. By combining these data with detailed information from animal studies the cumulated activity of the radiopharmaceutical and the resulting absorbed doses can be calculated more accurately. Although the calculations are based on a “virtual” standard patient, accurate dose calculation is important when estimating the long-term side effects on patients undergoing nuclear medicine examinations.

For all patients undergoing radionuclide therapy, patient-specific dose planning of the target volume (tumour) should be done and the absorbed dose to the non-target tissues should be kept as low as reasonable achievable (7,8). The absorbed dose to the tumour has to exceed a certain level to achieve the intended biological effect, a level that is tumour dependent. It is not always possible to obtain a therapeutic effect on the tumour because normal organs receive high absorbed doses that may lead to serious side effects. For instance, effects on bone marrow, such as acute myeloid leukaemia and myelodysplastic syndrome, have been reported (9), and also renal dysfunction (10-13), after radionuclide therapy. Biological effects on the liver, lungs, kidneys and

intestinal tract due to high absorbed doses have also been reported(10-16). The radiation sensitivity of normal tissues is thus a dose-limiting factor in radionuclide therapy, as it is in external radiation therapy.

Considerable efforts have also been made in establishing a correlation between the absorbed dose and the biological effects on tumours and normal tissue (17-19). Examples of factors influencing the biological effects on tissue are the absorbed dose rate, inhomogeneous activity uptake in tissue, and previous treatments (20,21). It has thus been found to be difficult to achieve reliable correlations. Despite this, it is still important to improve every step in the process of activity quantification and in calculating the absorbed dose at all tissue levels ranging from organs down to cell and subcellular levels, to obtain appropriate correlations (22).

Planar scintillation camera imaging (23-27) has so far been the most commonly used method for measurements of the time-activity distribution since it is less time and resource consuming than SPECT (single-photon emission computed tomography) or PET (positron emission tomography) imaging. Activity quantification from these images requires accurate corrections for scatter and attenuation, and in planar imaging the problem of activity in overlapping tissues can introduce considerable errors into the activity quantification. Calculations of the absorbed dose are based on dosimetric models of the body and its various organs. In the case of patient-specific dosimetry for an individual, these models have to be as close as possible to the patient anatomy. In addition, the accuracy is improved if the model reflects the structure of the organs or tissues, and can take into account the location of particularly sensitive cells.

The Aim of the Present Investigation

The general aim of this work was to investigate new methodologies in internal dosimetry to increase the understanding concerning factors that can affect the quantification procedure from planar scintillation camera images. In order to obtain more accurate dosimetry models and S values, the approach was to use a combination of detailed biokinetic data from animals and Monte Carlo simulations, to be used in anthropomorphic phantoms on macro level, and applied in the development and refinement of an intestinal dosimetry model on a small-scale level.

The specific aims were:

- to investigate the accuracy of the activity quantification procedures based on planar scintillation camera images concerning scatter correction methods and the influence of overlapping organ activity,
- to compare calculated absorbed doses using phantom-specific S values with absorbed doses obtained from the standard methodology using tabulated MIRD S values, and
- to develop an internal dosimetry model for the small intestine for calculation of the absorbed dose to the radiation-sensitive crypt cells from a radionuclide distribution in both intestinal wall and contents.

The Basics of Internal Dosimetry

The mean absorbed dose to an organ from an internally administered radiopharmaceutical is dependent on the characteristics of both the radionuclide and the pharmaceutical in terms of the type of radiation emitted and the spatial and temporal distribution of the radionuclide in the body. The mean absorbed dose, \bar{D} (Gy) can be calculated using the MIRD formalism (28) and the equation:

$$\bar{D} = \tilde{A} \cdot S \quad (1)$$

Here, \tilde{A} is the cumulated activity (MBq s), expressing the total number of decays during a particular time interval, and S is the mean absorbed dose to the target organ per unit cumulated activity in the source organ ($\text{Gy MBq}^{-1} \text{s}^{-1}$). The S value thus takes into account all physical factors when calculating the energy absorbed by the target organ, from radiation emitted from the source organ. Practical applications may, however, introduce several uncertainties. One such uncertainty is that the calculation of the mean absorbed dose is often based on the assumption that the radionuclide is uniformly distributed in the source volume. Also, human dosimetric models are of average size, although versions that are age- and sex-specific are available.

For radiation protection purposes in diagnostic applications, human models are relevant in absorbed dose calculations because the purpose is to estimate the risk of late stochastic effects on a large population of patients undergoing the same type of examination. The use of dosimetry factors based on a standardized phantom and average-based biokinetics is thus justified. The discrepancy between the body geometry of the patient and that of the dosimetry model and the individual variation in time-activity biodistribution introduce inaccuracies into the absorbed dose calculation. However, these are less important at least compared with the therapeutic situation (29).

When administering high activities for therapeutic purposes the aim is to produce sufficient deterministic effects on tumour cells but to avoid such effects on normal tissues. Therefore, the planning of radionuclide therapy is very important to ensure that the correct activity is administered to achieve the desired effect. The calculation of organ absorbed doses in patient-specific radionuclide therapy dose planning (19,30-33) has to be as accurate as possible, and hence the errors and uncertainties in the models have to be reduced.

For radionuclides emitting low-energy electrons a non-uniform activity distribution within the organ or tissue can give large variations in the absorbed dose to different cells or areas in the organ. Studies have shown that a small fraction of the cells in an organ can receive up to 15 000 times the average electron dose to the whole organ (34,35). This illustrates the importance of developing small-scale anatomy models for more accurate internal dosimetry.

In patient-specific dosimetry, both a patient-specific physical model as well as patient-specific biokinetic data should be included. If the inhomogeneous activity distribution within an organ or tissue could also be accounted for, the accuracy in the absorbed dose calculation would increase.

The Basics of the Monte Carlo Method

The Monte Carlo method is used to numerically solve problems that involve stochastic processes. The method has been continuously developed, and has become increasingly important and useful as computing power has improved. Monte Carlo simulations make it possible to calculate parameters that can not be measured in an experimental or a clinical situation. The method has been used extensively throughout this work and therefore a brief introduction will be given below. More detailed information about the method can be found in the review papers by Andreo (36) and Zaidi (37).

Principles

The principle behind the Monte Carlo method when used in radiation physics is to simulate the radiation transport through a medium by calculating the track of each particle and determining the fate of the particle based on probability distributions. The various interactions that can occur are determined using uniformly distributed random numbers. These numbers, often normalized within [0-1], then determine, for example the path length, scattering angle and type of interaction on the basis of differential probabilities.

Photon Simulation

Photons are relatively easy to simulate since they interact with matter in a few well-defined ways: the photoelectric effect, Compton scattering, coherent scattering and, for energies at and above 1.022 MeV pair production. Simulations also often include secondary photons, such as characteristic X-rays and bremsstrahlung.

Charged-Particle Simulation

Charged particles (such as electrons) interact with matter through several different mechanisms. Some of these interactions lead to "catastrophic" events involving large deflection angles and significant loss of energy. These interactions include large energy loss by electrons and positrons, hard bremsstrahlung emission and electron-positron annihilations. However, several types of interaction types result only in small deflections and minor energy loss. These include low-energy electron scattering atomic excitations, soft bremsstrahlung emission and elastic electron multiple scattering from atoms. Since the number of interactions for these "non-catastrophic" events is

very large, explicit simulation of each process is not practical. To reduce the calculation time many electron interactions can be grouped together. Statistical theories have been developed to describe these “weak” interactions by accounting for them in a cumulative way and these are called “statistically grouped” interactions.

Public-domain Programs

Several extensive and accurate programs have become publicly available. Examples are the SIMIND code (38) and the SIMSET code (39,40) for the simulation of scintillation camera imaging and SPECT/PET. These have been widely used in diagnostic nuclear medicine to investigate the characteristics of scintillation camera systems and to determine un-measurable parameters such as the scatter in the image (41-44). This is possible since every detail of the transport chain is known and the type of particle can be easily classified (scattered photon, primary, un-attenuated etc.).

The evolution of charged-particle programs started with the development of the ETRAN code by Berger and Seltzer (45,46). Parallel with this the Electron Gamma Shower (EGS) system was developed at Stanford Linear Accelerator Centre (47). A later version, EGS4, included routines and data for the simulation of energy ranges useful in medical radiation physics. The accuracy of EGS4 was also improved by the PRESTA algorithm which adjusts the step length of a condensed history as the particle comes close to a boundary.

Another Monte Carlo code often used in dosimetry calculations is the Monte Carlo N-Particle (MCNP) code (48), which also includes neutron simulations. This program has a combinatorial geometry package that allows complex geometries to be built up based on simple geometries.

Geant4 is a program developed at the CERN Nuclear Physics Research Centre in Geneva. It is mainly used for high-energy physics and the design of new detectors, but a consortium called OpenGate (49), has developed routines to use Geant4 for medical applications which have proven to be very flexible in the design of new SPECT and PET systems (50).

Phantoms

The Monte Carlo method is the main tool used to calculate dose conversion factors. Based on a standardized geometry, the transport of energy by photons and electrons is simulated and source-to-target dose factors are calculated by an accurate coupled electron/photon program.

When using Monte Carlo programs in medical applications the accuracy in the simulated phantom can be critical. The internal shapes of organs in a human are very complicated, and the assumption of equivalent cylinders is not always justified. The realistic anthropomorphic phantoms recently developed are therefore of great importance. These phantoms are often represented as voxel matrices where the value of each voxel represents an activity (or density) and its position in the 3D matrix represents its location (x,y,z) in the Cartesian coordinate system. By linking a voxel value to a specific material one can simulate non-homogeneous attenuation. The phantom matrix can also be obtained from a computed tomography (CT) study of a specific patient, leading to very accurate simulation for a specific case.

Several voxel-based phantoms have been developed for general purposes (51-55). One of the earlier phantoms is the thorax and the brain phantoms developed by Zubal et al. (51). These phantoms were obtained from detailed CT images (thorax) and magnetic resonance (MR) images (brain) in which the structures and organs were segmented, slice-by-slice, and assigned a unique code that identifies each voxel. From these codes, an activity or density distribution can be generated and used in a Monte Carlo program. Another group of useful voxel phantoms is the MCAT/NCAT phantom family (56,57). These voxel phantoms are completely mathematical and the user can, to some extent, modify the phantom shape in a parameter file. In the NCAT phantom, respiratory motion can be included, as well as physiological heart motion.

Activity Quantification

The cumulated activity, \tilde{A} , in Eqn (1) can be written as the time integral of the activity, A_b , in the source organ, b , during the time interval of interest.

$$\tilde{A}_b = \int A_b(t) dt \quad (2)$$

Several methods are available to acquire information on the temporal change in the radionuclide biodistribution, e.g. scintillation camera imaging, discrete probe monitoring, tissue sample counting and excreta collection. In addition to human studies, animal studies are very useful in gaining more knowledge and identifying tissues in which the radiopharmaceutical is accumulated and the excretion paths (58,59) in a controlled way. It is important to collect sufficient information concerning the activity uptake and to determine the elimination rates in the organs of interest in order to plan patient-related dosimetric studies in an appropriate manner. Too few sampling points or inappropriate time intervals between the points could lead to inaccurate results. In general, three or more time points are required for each uptake or elimination phase in order to be correctly fitted by an exponential function (58).

The Scintillation Camera

A convenient and relatively simple method for activity quantification is the use of scintillation cameras to obtain planar images of the radionuclide distribution in the body at various points in time. Several aspects regarding the design of the camera and the way in which images are created must, however, be considered to ensure accurate activity quantification from scintillation camera images. Corrections have to be made for, e.g., the photon attenuation and the contribution to the image from photons scattered in the patient and in the camera system, the detector sensitivity and, for some radionuclides, possible penetration through the septa walls in the collimator. In radionuclide therapy count rates may be high during the early phase of treatment, which may result in count losses and potential mis-positioning of events in the image due to camera limitations. On the other hand, a low count rate can be a problem later on leading to high statistical uncertainties and noisy images (21).

Today, most scintillation cameras are optimized for $^{99}\text{Tc}^{\text{m}}$ and have relatively thin NaI(Tl) crystals. The increasing use of radionuclides that emit photons of higher energies, e.g. ^{131}I and ^{111}In , can lead to additional imaging problems. For example, the principal photon energy of ^{131}I is 364 keV (81% per disintegration) but additional photons are emitted, two having energies of 637 keV and 723 keV. The abundance is low (7.2% and 1.8%) but because of the high energy, septal penetration will be a serious problem, resulting in degraded spatial resolution in the image. Software correction can be made or an ultra-high energy collimator can be used to reduce the level of septal penetration. In addition to septal penetration, events in the image originating from back-scattering in light guides, PM tubes and the camera housing can also contribute to the events acquired in the window defining the principal photon energy (60).

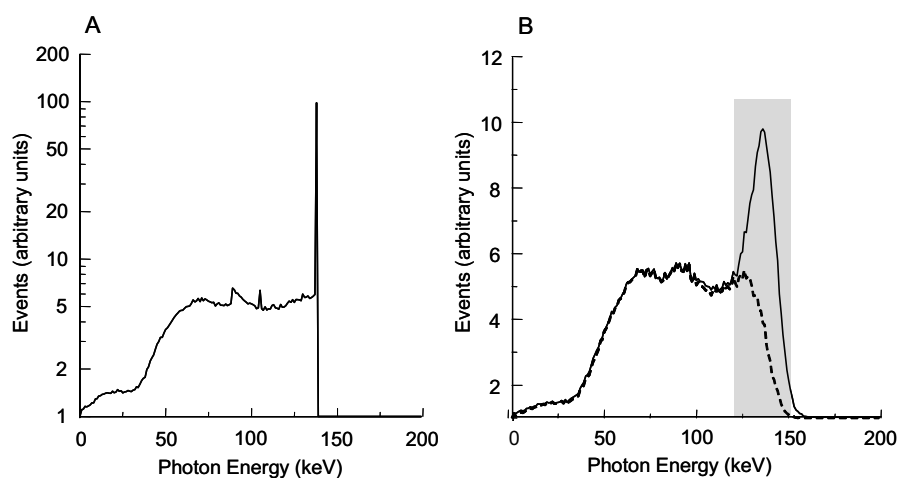


Figure 1. Simulated energy spectra for $^{99}\text{Tc}^{\text{m}}$ in a water phantom are shown in the figure. The true energy deposition in the scintillation camera crystal is seen in A) and the measured energy deposition in B). The shaded area represents a 20% energy window and the dotted line shows the contribution due to scattered photons. The number of primary photons detected in the photopeak is the same in Figure A) and B).

One of the major problems in scintillation camera imaging is that some of the photons scattered in the patient will still have an energy accepted by the energy window and therefore contribute to the image. Figure 1A shows a simulation of the energy deposition in a scintillation camera crystal. For a perfect scintillation camera the measured spectrum (Fig. 1B) would have been identical to 1A, but due to statistical variations in the light emission,

transmission and collection, and also statistical variations in the PM tube response, the measured energy deposition peak is broadened. This energy resolution, measured as the FWHM, is of the order of 8-10% at 140 keV for modern cameras. In order to collect a sufficient number of primary photons a relatively wide energy window is needed which results in the registration of scattered photons.

A disadvantage of planar scintillation camera imaging, however, is that the resulting 2D representation of the *in vivo* 3D activity distribution leads to quantification problems due to activity in overlapping tissues in the planar images. When using SPECT this problem is greatly reduced and the organ activity concentration and, in some cases, the organ volume, can be accurately determined (58). SPECT studies are, however, time consuming and the field of view is limited, so planar imaging techniques remain the most commonly used methods despite their known problems.

Planar scintillation camera imaging does not provide information about the volume of the organ or tumour so these have to be obtained by morphological methods, such as CT studies or MR imaging. It should, however, be remembered that volumes obtained by these techniques do not necessarily correspond to the volume of the physiologically active part of the tissues. This potential overestimation of the organ volume, and hence the mass, can result in underestimation of the mean absorbed dose to an organ. An inhomogeneous activity uptake may lead to under- or overestimation of the absorbed dose in sub-regions of the organ relative to the mean absorbed dose for the whole organ.

The Conjugate-View Attenuation Correction Method

The most commonly used collimator is the parallel hole collimator. An important collimator parameter is the geometrical sensitivity (i.e. the number of photons passing through the holes divided by the number of photons emitted). The geometrical sensitivity is independent of the distance when imaging a source in air. Thus, the determination of the calibration factor (cps MBq⁻¹) is often straightforward for a particular camera configuration. However, when measuring activity in patients, photons will be attenuated in a way that depends on source distribution and body composition. The calibration factor will therefore be highly dependent on the particular study and patient. Correction for this attenuation is therefore necessary.

A commonly used method for attenuation correction in planar scintillation camera images is the conjugate-view method (23-25). This method is fairly

accurate for geometrically well-separated activity sources with negligible activity in surrounding tissues. Advantages of the method are that it does not require any information on the depth of the source and the measurements are relatively easy to perform.

Two opposite scintillation camera images of the patient or part of the patient are acquired, usually the anterior and posterior view. For a point source located at a depth d , in a medium with the attenuation coefficient, μ , the number of counts detected in the anterior view, C_A , and posterior view, C_P , is given by:

$$C_A = C_0 e^{-\mu \cdot d} \quad (3)$$

and

$$C_P = C_0 e^{-\mu \cdot (L-d)} \quad (4)$$

where L is the thickness of the patient for the particular section and C_0 is the count rate that would have been obtained if the source had been unattenuated. If the geometric mean of C_A and C_P is calculated:

$$\sqrt{C_A \cdot C_P} = \sqrt{C_0^2 \cdot e^{-\mu L}} \quad (5)$$

the result will be independent of the source depth. The activity can be calculated from the system sensitivity obtained in air, K (cps MBq⁻¹).

$$A = \frac{C_0}{K} = \frac{\sqrt{C_A \cdot C_P}}{K \cdot e^{-\mu \frac{L}{2}}} \quad (6)$$

The attenuation coefficient used for patients is a weighted sum of the coefficients $\sum_i \omega_i \cdot \mu_i$ for all tissues, i , along the projection. This weighted sum of attenuation coefficients can be measured using a radioactive flood source on the opposite side of the patient, and making measurements with the scintillation camera, with and without the patient. A transmission factor image can then be obtained by calculating the ratio between these measured

images on a pixel-by-pixel basis. Recent camera systems including an X-ray device also allow for fast and accurate transmission measurements (61,62).

It should be remembered that Eqns (2) and (3) only are valid for a point source. For a distributed source (as is often the case) the source organ thickness can be taken into account by the additional term in Eqn (6):

$$A = \frac{C_0}{K} = \frac{\sqrt{C_A \cdot C_P}}{K \cdot e^{-\mu \frac{l}{2}} \cdot \frac{\sinh(\mu \cdot l/2)}{\mu \cdot l/2}} \quad (7)$$

in which l is the source thickness. The correction for source organ thickness can only be used for well-defined sources (63), but since the activity distribution in the body changes with time the source thickness and the magnitude of the correction term should also be a function of time and preferably also of the part of the body in question. This was taken this into consideration in the calculations presented here.

For the case of a small source located close to the surface, or in areas with high background activities, meaning that the activity is only detectable in one of the two conjugate views, the use of the “effective point source method” may provide more accurate activity quantification (58,64-67). In this method a broad-beam value for the attenuation coefficient, here denoted the effective attenuation coefficient, μ_e , is used as a quantitative compensation for attenuation due to the scattered photons. Knowing this effective attenuation coefficient the system sensitivity and the depth of the source, the activity can be calculated using data from only the anterior or posterior measurement, C_x . The expression is reduced to:

$$A = C_x e^{\mu_e d} F / K \quad (8)$$

where F is the background correction.

Measurement of Attenuation Coefficients

The methods used for transmission measurements are often based on an external radionuclide source in the form of a scanning line source or an uncollimated flood source. The drawback of using an uncollimated flood source is the broad beam geometry, leading to the detection of many scattered photons (68). If these attenuation data are used in combination with a scatter correction of the emission data, the activity obtained from the corrected image

will be underestimated. Collimation of the transmission source would create a more narrow-beam-like geometry and thus reduce these problems. The transmission measurements will then provide a more relevant transmission map for this particular photon energy. However, if the photon energy of the external source is close to the energy of the administered radionuclide, it can be regarded as being representative of the emission study. Using CT for the transmission study requires recalculation of the attenuation values for them to be valid for the emission photon energy.

The increasing use of hybrid systems SPECT/CT and PET/CT provides many advantages. The high photon fluence rate from CT provides transmission scans with good statistics in less than a minute. The short acquisition time is, however, also a disadvantage as breathing for example, will blur the contours of the lungs in the emission study but not in the transmission study, resulting in artefacts in the attenuation-corrected image, which must be corrected for.

Correction for Scatter

For photon energies commonly used in nuclear medicine the attenuation is mainly due to Compton scattering. Less than 1% of the interactions in soft tissue with the 140-keV photons from ^{99m}Tc is due to the photoelectric effect. In image acquisition an energy window between 15% and 20% in width (FWHM) is often used to ensure good statistics and reasonable acquisition times. These relatively large windows are necessary because of the limited energy resolution of scintillation cameras (~8-10% FWHM at 140 keV). The result of using these wide windows is that scattered photons will also be detected and included in the image. Using the conjugate-view method with linear attenuation coefficients and no compensation for scatter thus results in overestimation of the activity. To improve the accuracy of the activity quantification and the image quality, scatter correction is needed and various methods have been reported and investigated. These include the use of:

- additional energy windows to estimate the amount of scattered photons included in the energy window centred over the photopeak (69-74),
- an effective attenuation coefficient, μ_s , to prevent overcorrection in the attenuation correction due to the presence of scattered photons (75-78)
- buildup factors to describe the scatter (79-84),
- Fourier image restoration using a modified Wiener filter (61,85),
- convolution/subtraction methods (86,87), and
- energy-weighted acquisition (88-90).

The methods used in the current work are described below together with the commonly used buildup factor method.

The Effective Attenuation Coefficient

An effective attenuation coefficient, was used by Thomas et al. (75) in the conjugate-view method to correct for scattered events by reducing the magnitude of the attenuation correction. Values of the effective attenuation coefficient, were empirically determined to be in the range of 0.12-0.142 cm⁻¹ for ^{99m}Tc in the patient (75-78,91-93) and these were used for quantification of both planar and SPECT images. This simple method works well in objects with uniform attenuation and uniform radionuclide distributions. It does not, however, account for the spatial distribution of the scattered events, especially when imaging the thorax region, where large variations in tissue composition and density are present (94).

The Buildup Factor Method

Wu and Siegel (79) have developed a method based on pre-calculated buildup factors for scatter correction. The buildup factor, $B(d)$, is defined as the ratio:

$$B(d) = \frac{C}{C_0 \cdot e^{-\mu d}} \quad (9)$$

where C is the count rate measured for a source at a depth, d , in a phantom, C_0 is the count rate in air and μ is the linear attenuation coefficient. Separate measurements of the buildup factor (or calculations using the Monte Carlo method) are needed as this factor is dependent on the radionuclide, the depth and distribution of the source, energy window width and energy resolution. The variation in $B(d)$ is, however, relatively small even for large differences in source area.

For a point source the measured counts in the anterior view, C_A , and the posterior view, C_P , can be described by:

$$C_A = C_0 B(d) e^{-\mu d} \quad (10)$$

and

$$C_P = C_0 B(L-d) e^{-\mu(L-d)} \quad (11)$$

where L is the object thickness. For an extended source the photon attenuation within the source volume (self-attenuation) is included in the equations, giving:

$$C_A = C_0 B(d) e^{-\mu d} \left[e^{\mu l/2} \frac{(1 - e^{-\mu l})}{\mu l} \right] = C_0 B(d) e^{-\mu d} \left[\frac{\sinh \mu l / 2}{\mu l / 2} \right] \quad (12)$$

and

$$C_P = C_0 B(L-d) e^{-\mu(L-d)} \left[e^{\mu l/2} \frac{(1 - e^{-\mu l})}{\mu l} \right] = C_0 B(L-d) e^{-\mu(L-d)} \left[\frac{\sinh \mu l / 2}{\mu l / 2} \right] \quad (13)$$

where l is the thickness of the source organ. Knowing this thickness and assuming that the depth, d , is $L/2$, the buildup factor $B(L/2)$ can be used to solve the equations for C_0 and d . The corresponding buildup factors are determined for this new depth and the iterative procedure is repeated until C_0 converges. For activity determination this method requires, in addition to the pre-determined tabulated buildup factors, only C_A , C_B , L and the system sensitivity, K , of the camera.

Siegel et al. (81) modified the buildup factor method by using a buildup factor for infinite depth, $B(\infty)$, which is independent of source depth for a given energy window and valid only for a thin source. The fraction of un-attenuated photons can be calculated as the ratio between C and C_0 . According to Wu and Siegel (79), this ratio can then be described as

$$C / C_0 = 1 - (1 - e^{-\mu d})^{B(\infty)} \quad (14)$$

The depth-independent buildup factor $B(\infty)$ (DIBF) is determined as the pseudo-extrapolation number of the linear part of the semi-log plot of the relative fraction of un-attenuated photons as a function of source depth. The count rates in anterior and posterior views for this DIBF method can then be described by

$$C_A = C_0 \left[1 - (1 - e^{-\mu d})^{B(\infty)} \right] \left[\frac{\sinh \mu l / 2}{\mu l / 2} \right] \quad (15)$$

and

$$C_P = C_0 \left[1 - (1 - e^{-\mu(L-d)})^{B(\infty)} \right] \left[\frac{\sinh \mu l / 2}{\mu l / 2} \right] \quad (16)$$

The depth, d , can be calculated numerically by using the ratio of C_A and C_p

$$C_A / C_p = \left[1 - (1 - e^{-\mu(d)})^{B(\infty)} \right] / \left[1 - (1 - e^{-\mu(L-d)})^{B(\infty)} \right] \quad (17)$$

and by varying the value of d ($0 \leq d \leq L$) and using the expression for C_A or C_p to calculate C_o . The activity is then obtained by using the system sensitivity. If the depth is known, C_o can be calculated from the expression for C_A directly. The variation in μ with source size and $B(\infty)$ must be pre-calculated for each scintillation camera system to make use of the DIBF method for scatter correction.

The Triple-Energy Window Method

The triple-energy window (TEW) scatter correction method was first introduced for SPECT (60,95), but is also useful for planar imaging (26,96,97). The scatter correction is performed pixel-by-pixel by subtracting the estimated number of scattered counts from the measured total counts. One energy window is placed over the photopeak using a window width appropriate to the energy resolution of the camera system. Two much narrower windows are placed on either side of this window and used to estimate the fraction of scattered photons included in the photopeak window.

The number of primary attenuated photons detected, C_{prim} , is given by:

$$C_{prim} = C_{total} - C_{scat} \quad (18)$$

where C_{total} is the total number of photons detected and C_{scat} is the number of scattered photons detected in the window. It is not possible to measure C_{scat} but it can be estimated using C_{TEW} , which is calculated from:

$$C_{TEW} = \left(\frac{C_l}{W_l} + \frac{C_u}{W_u} \right) \cdot \frac{W_m}{2} \quad (19)$$

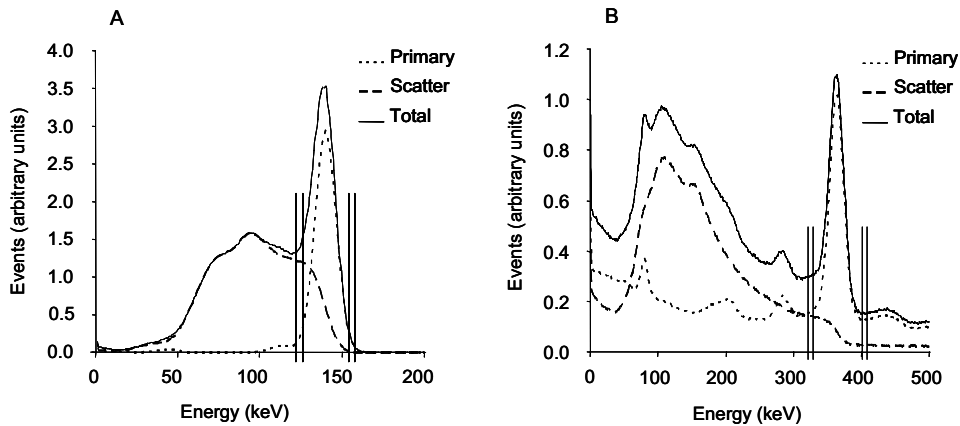


Figure 2. The simulated energy spectra for A) ^{99m}Tc and B) ^{131}I showing the energy windows used in the triple-energy window method for scatter correction.

where W_l and W_u are the widths of the lower and the upper energy windows, respectively, and W_m is the width of the main window centred over the photopeak. The scatter windows include scatter and events caused by septal penetration of photons with higher initial energies than the principal photon energy. The energy windows used in these simulations are shown in Figure 2. Figure 3 shows simulated images of the biodistribution of ^{99m}Tc -sestamibi using different energy windows compared with the ideal image without scatter and attenuation (Fig. 3A) and the normal image (Fig. 3B). The lower energy window (Fig. 3C) contains scattered photons mainly of the principal energy but also scattered and septal penetration from higher-energy photons. For radionuclides emitting photons of a single energy, such as ^{99m}Tc , only a few events will be detected in the upper energy window (Fig. 3D) mainly due to the limited energy resolution. The scatter windows should be narrow enough to represent the scatter detected in the photopeak, but wide enough to avoid large statistical uncertainties in the final scatter estimate. The scatter estimate (Fig. 3E) is then subtracted from the measured data (either pixel-by-pixel or ROI-by-ROI) prior to the attenuation correction. Comparison of the calculated image (Fig. 3E) and the true image of the scattered events (Fig. 3F) shows a good agreement.

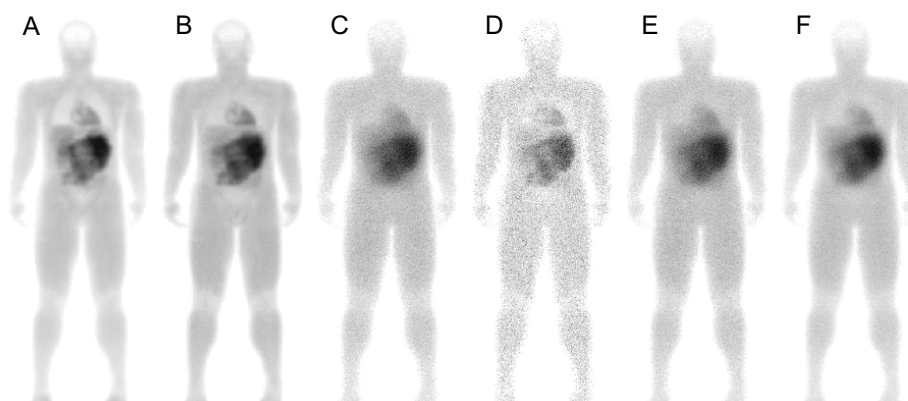


Figure 3. Simulated images showing the biodistribution of ^{99m}Tc -sestamibi, 2 h after injection. The images show: A) the ideal image without scatter and attenuation, B) the “normal” image including scatter and attenuation, C) the image with the lower energy window and D) the image with the upper energy window used in the TEW method, E) the sum of the lower and upper energy windows and F) the true image of the scattered events.

Definition of Regions of Interest

Accurate quantification of the activity uptake in an organ or a tumour is determined not only by the quantification method used but also by how the regions of interest (ROIs) are defined. The optimal method for a ROI determination should be easy to perform, automatic, reproducible, user-independent and relatively insensitive to partial volume effects (98). An often used category of methods is that based on a threshold, where regions are automatically defined at a certain threshold level of the maximum value within the organ or lesion. This threshold can either be fixed (e.g. 50%) or calculated using a grey-level histogram method (99). This method is relatively independent of source size and geometry, as long as the size of the source is larger than twice the spatial resolution of the camera system. Sources smaller than this will be underestimated in size and activity due to the partial volume effect (100). In planar and SPECT imaging this effect is often described in terms of “spread” or “blur” of the regional activity uptake due to the displacement of counts (“spill-out”) into an area outside the defined ROI. “Spill-in” or “spillover” of counts from the background activity into the ROI can also be included. The importance of this effect depends on the size and proximity of the background activity in relation to the ROI and is an effect of the finite spatial resolution and sometimes collimator septal penetration (101).

Background Activity Correction

In a planar scintillation camera image, the organ of interest is seldom separated completely from other tissues with activity uptake, and therefore the contribution to the acquired number of counts in the ROI originating from photons emitted from from over- or underlying tissues (often denoted “the background”) must be addressed. This contribution can originate from circulating activity in the blood, activity in the extracellular fluid and soft tissue as well as activity in overlapping organs and tissues. Different methods of background correction have been proposed (75,83,102). The simplest background correction method is based on using a ROI appropriately placed adjacent to the organ ROI. The number of counts per pixel in that background ROI is subtracted from the counts per pixel in the organ ROI. This method will, however, overestimate the background as it does not consider the actual organ thickness (102). Thomas et al. (75) presented a method that takes into account the thickness of the organ and the background volumes above and below the organ, and the method also includes effects of different attenuation coefficients in different layers in the region of interest. A background correction method was proposed in a study by Kojima et al. (83) where the volume occupied by the organ was considered when the organ and body thicknesses are known. In this method the organ depth is also used to calculate the actual fraction of background counts from tissues over and under the organ. A simplified method was proposed by Buijs et al. (102) in which only the organ thickness, l , and body thickness, L , are required. Here, the fraction of the total background activity, F , is calculated by:

$$F = 1 - (l/L) \quad (20)$$

The method described by Kojima et al. is the most accurate according to a study by Buijs et al. (102). The method proposed by Buijs et al. is also accurate but is more sensitive to low organ-to-background activity concentration ratios (i.e. ratios close to 1). The Buijs method was used for background corrections in the studies described in **Papers III and IV**.

Activity in Overlapping Tissues

A 2D representation of the activity distribution in a patient can lead to problems in organ activity quantification due to contributions from activity distributions in overlapping tissues. An example of this is described here based on the work presented in **Paper III**. Figure 4 shows simulated images of the total activity distribution and the activity in some separate organs. ROIs covering parts of the kidneys are also shown.

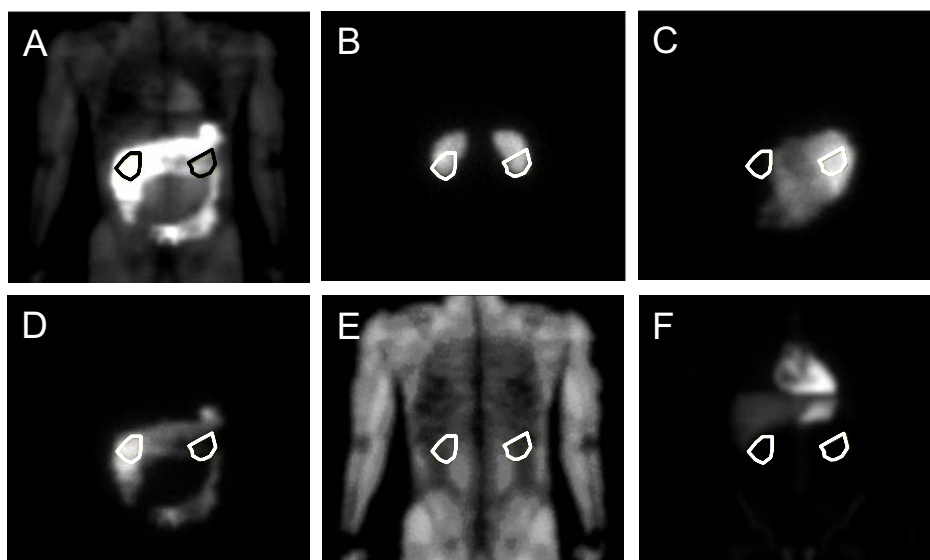


Figure 4. Simulated ^{99m}Tc images showing activity distributions of ^{99m}Tc -sestamibi 6 h after injection: A) the total activity, B) the kidneys, C) the small intestine, D) the colon, E) the skeletal muscles and F) the rest of the organs. ROIs are shown over parts of the kidneys. The image intensities are not interrelated.

Figure 5 shows the contribution in small parts of the right and left kidneys from overlapping tissues. During the first few hours after injection of this radiopharmaceutical activity quantification and ROI analysis over the right kidney is preferable to the left kidney because of the relatively high activity uptake in contents of the small intestine. During the transport of activity into the colon, the inaccuracy in activity quantification determined by a ROI over the right kidney increases and results in greater overestimation of the activity compared with using data from the left kidney 6 to 24 h after injection. The contribution of counts in the kidney ROI from the colon was found to be as high as 60 times the contribution from the kidney itself.

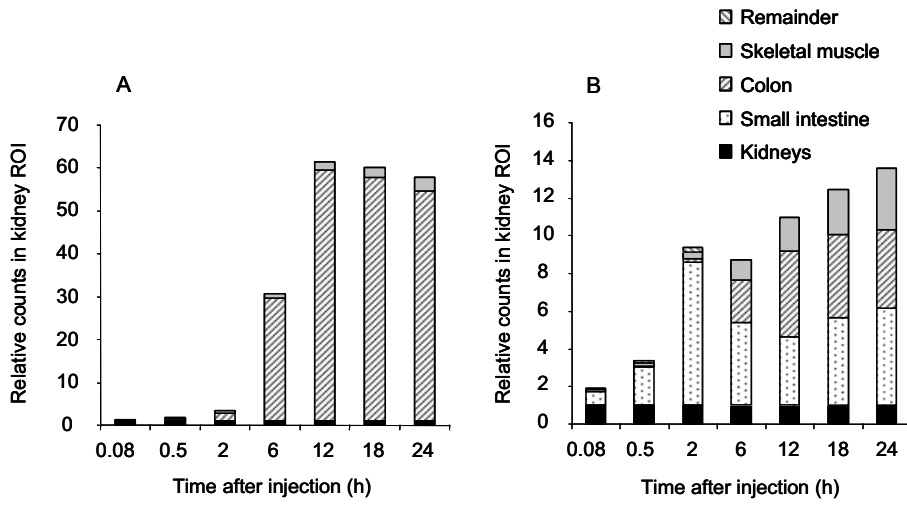


Figure 5. The activity contribution to A) right and B) left kidney ROI from activity in overlapping tissues.

The Absorbed Dose Conversion Factor

As shown in Eqn (1), the absorbed dose depends on both the cumulated activity and the absorbed energy fractions of particles emitted by a source volume to a target volume. The dose conversion factor is given by

$$S_i(r_k \leftarrow r_h) = n_i E_i \frac{\varphi(r_k \leftarrow r_h)}{m_k} \quad (21)$$

where n_i is the number of photons or particles with the mean energy E_i , and $\varphi(r_k \leftarrow r_h)$ is the fraction of the energy emitted by the source organ, r_h , that is absorbed in the target organ, r_k , and m_k is the mass of the target organ.

The absorbed energy fraction is generally impossible to measure *in vivo* and, therefore, geometrical models of humans have been developed, which together with a Monte Carlo program, make it possible to calculate the absorbed fraction of energy per particle for a particular radionuclide. The accuracy in the calculation of the absorbed dose to a target volume is then of course highly dependent on how detailed and realistic the model describes the organs and tissues within a human.

General Geometrical Models of the Human Body

The MIRD committee presented an anthropomorphic phantom of the human body in MIRD pamphlet No. 5 revised (6). The mathematical representation of the human body and several organs consisted of geometric shapes such as cylinders, spheres, cones and ellipsoids. This phantom was used to simulate absorbed fractions for photons and S values for several radionuclides given in MIRD pamphlet No. 11 (103) using Monte Carlo simulations.

Developments have led to a set of more realistic phantoms, the Oak Ridge National Laboratory (ORNL) phantoms, including an adult male (although hermaphroditic) five phantoms representing children of different ages (newborn, 1, 5, 10 and 15 years old) (104) and four adult women, one of which is non-pregnant and the other three are at different stages of pregnancy (105).

Further developments have resulted in dosimetry models for the heart chamber and wall (106), urinary bladder (107), head and brain (108) and the kidneys (109). Also, a dosimetry model for voxel sources has been presented in MIRD pamphlet No. 17 (110). Other organs and tissues of special interest for

absorbed dose calculations have been modelled, such as the eye, peritoneal cavity, prostate gland, bone, rectum and small spheres representing tumours or organs in a small animal. These models have been reviewed by Stabin (111). Dosimetry models of the small intestine have also been presented and some of them are summarized below.

Han et al. (112) recently presented a revision of the ORNL series of computational phantoms. This revision includes several improvements, e.g. new models of the head, brain, kidneys, rectosigmoid colon and a new model of the mucosal layer of the intestinal tract. New reference values for elemental tissue composition and mass densities (113,114) are used and a method for deriving patient-specific, specific absorbed fractions for both electrons and photons has been proposed. Using the stomach mucosa as an example, they showed that the absorbed dose calculated with the currently used MIRD schema is overestimated by up to several orders of magnitude for electron energies below 1 MeV. The models also take into account the possibility of activity uptake in the mucosal layer.

A computer program, MIRDOSE (115), has been developed to facilitate and automate absorbed dose calculations in nuclear medicine (116). MIRDOSE version 3 is based on the six ORNL adult and child phantoms (104) and the four adult pregnant and non-pregnant women phantoms (105). The methods in MIRDOSE program together with a curve-fitting algorithm for kinetic data have been included in the new OLINDA/EXM program (116). The new models for the peritoneal cavity (117), prostate gland (118), head and brain (108) and kidneys (109) are included in the software.

Scaling of Dose Conversion Factors

The accuracy of the calculated absorbed dose is influenced by the discrepancy between the anatomies of the patient and the computer phantom used for S value determination. The flexibility of these values is limited to a selection based on gender and age. The absorbed dose calculations can, however, be partly adjusted to specific patients.

The organ self-dose from particles can be adjusted to the individual's organ mass by linear scaling of the S value according to:

$$S_{organ,patient} = S_{organ,MIRD} \frac{m_{organ,MIRD}}{m_{organ,patient}} \quad (22)$$

This assumes that the organ dimensions are much greater than the range of the emitted particle. In MIRD pamphlet No. 11 (103) it is concluded that when source and target are the same organ the absorbed dose from photons will be proportional to $m^{-2/3}$ where m is the mass of the target organ. This gives a scaling of the self-dose

$$S_{organ,patient} = S_{organ,MIRD} \left(\frac{m_{organ,MIRD}}{m_{organ,patient}} \right)^{2/3} \quad (23)$$

for photon energies above 100 keV (31,103,116). For source and target organs sufficiently separated, the S value does not change much as a function of the mass for photons (116). When the total body is the source organ the S value can be extrapolated using the mass ratio for the computer phantom and the mass of the particular patient (103) if one assumes that the organ masses follow the total body mass or, more realistically, the lean body mass. This scaling is based on the assumption that the variation in organ mass does not influence the absorbed fraction of emitted energy. Differences in the geometry of organs are, however, not yet easily accounted for neither is the radionuclide distribution within organs (31).

In **Paper IV** the S values calculated for the Zubal phantom are compared with the S values given for the adult male phantom in the OLINDA program. The results are shown in Figure 6A. The self-dose S values expressed as the ratio between the Zubal S values and the OLINDA S values are shown for some organs. Here, the mass correction described by Eqn 21 was used, since only the total S value for a radionuclide, i.e. contributions from both electrons and photons, for each source-target organ combination is available in the OLINDA program. The self-dose S values agree fairly well after correction, except those for the colon and the small intestine, probably due to differences in the models of the intestines. In the Zubal phantom all voxels included in the intestinal wall are regarded as being part of the intestine for both the colon and the small intestine, i.e. both wall and contents are included in the S value calculation.

The corresponding variations in cross-dose S values for various organs are shown in Figure 6B. Apart from the intestines, the ratio is in the range of 0.32 to 2.4. Stabin and Yoriyaz (119) have presented values for the specific absorbed fraction (SAF) for mono-energetic photons and they also found differences between Zubal phantom and MIRD phantom data. The differences may be due to overlapping organs in the Zubal phantom and differences in organ volumes. Zankl et al. (54) have found that the variation in

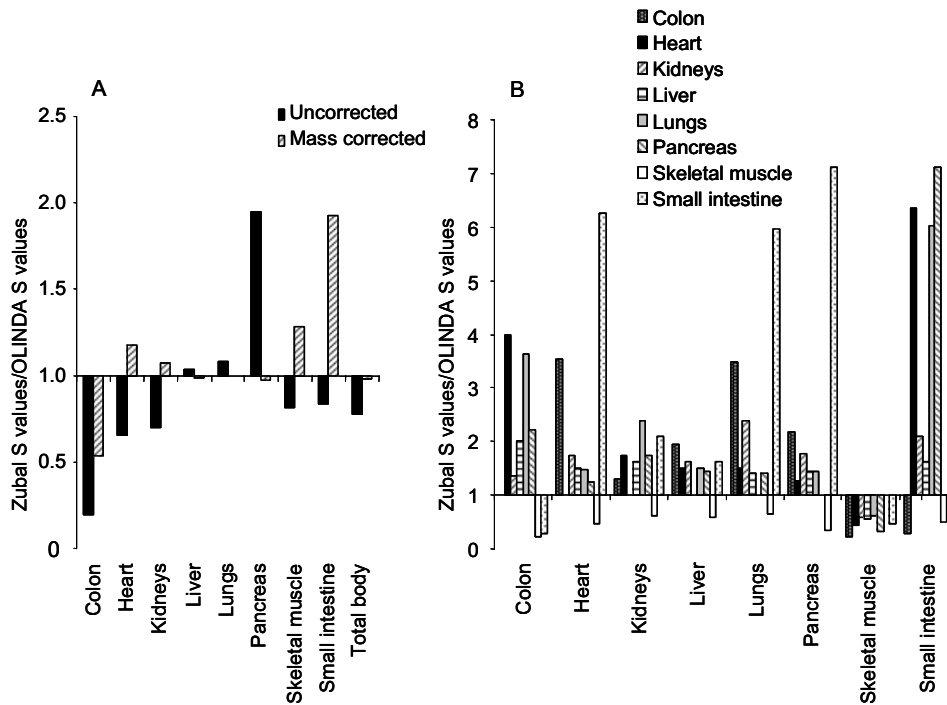


Figure 6. A) Ratio of self-dose S values for ^{99m}Tc (Zubal S values/OLINDA S values) for the different organ masses. B) Ratio of S values for ^{99m}Tc to the target organs on the x-axis given as the ratio between Zubal S values and the OLINDA S values.

SAF values between different types of realistic voxel phantoms is large and even larger when comparing results from these types of phantoms with results from the more stylized MIRD phantom. They concluded that these differences depend on the individual organ mass and variation in distance between organs.

Self-dose from β -emitting radionuclides, such as ^{131}I , is sometimes regarded as being equivalent to the electron dose, thus assuming the photon contribution to be negligible. In **Paper IV** it was shown that the photon contribution for ^{131}I in our application is significant and contributes about 5-15% of the total self-absorbed dose, and even more for large organs such as the liver, the small intestine and the muscles (25-30%). A full Monte Carlo simulation is then a useful tool for investigation of the influence of organ size and geometry for different radionuclides and activity distributions.

The Small Intestine as a Specific Case

In both diagnostic and therapeutic nuclear medicine, radiopharmaceuticals are used that may irradiate the radiosensitive intestinal wall. The administered radiolabelled substance can give an activity uptake in the intestinal wall, the activity can be excreted via the intestinal tract and the intestines also receive an absorbed dose from the activity in surrounding organs.

Patient studies using ^{90}Y -labelled monoclonal antibodies for radioimmunotherapy have been reported to give intestinal radiation effects observed as various grades of diarrhoea (12,120,121) and the administration of ^{223}Ra for pain palliation has been shown to lead to high absorbed doses to the intestinal tract (122,123). Indium-111 compounds have also been shown to accumulate in the intestinal wall (124). It has been suggested that the antibody uptake is caused by the targeting of antibodies to antigens expressed on the normal intestinal mucosa (120).

The studies described in **Papers I and II** are based on the biokinetics of $^{99\text{m}}\text{Tc}$ -sestamibi, investigated in animals. For this substance, 6% of the radiopharmaceutical had accumulated in the small intestinal wall 2 h after injection. The radiopharmaceutical is used for myocardial function studies which imply that the activity uptake was probably localized to the muscular layer of the intestinal wall. The intestinal tract is also involved in the excretion of the radiopharmaceutical, and 46% of the injected activity was eliminated from the body via the intestinal contents.

There is thus a need for a dosimetric model of the small intestine for accurate calculations of the absorbed dose to the sensitive cells in the intestinal wall. In order to improve the dosimetry for the small intestine and to account for different source locations, a dosimetry model for the intestine should thus include the possibility to localize the activity to various parts of the intestine, i.e. in the wall, in parts of the wall and in the intestinal contents. The cross-dose from activity in other parts of the intestinal tract should also be included.

It is difficult to create a realistic model of the small intestine, since the anatomy varies with different parts of the intestine. The intestine transports the contents by contracting movements, so there is also a variation in the dimensions over time. A change in model data can result in variation in the calculated absorbed dose to the crypt cells depending on the source location.

Figure 7 shows an illustration of the small intestine in the body and a cross-section of the small intestinal wall.

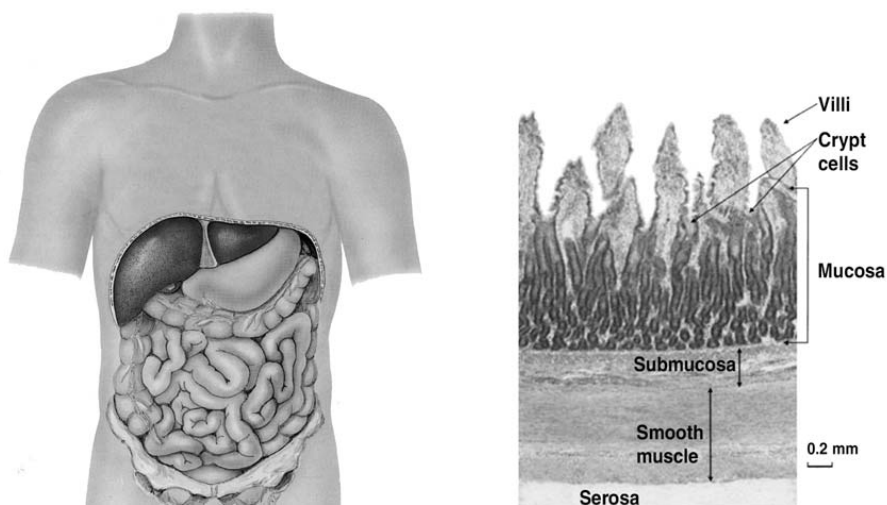


Figure 7. The small intestine in the body (left) and an enlarged histological cross-section of the small intestinal wall (right). (Reprinted by permission of Liber, Sweden, and the Mary Ann Liebert, Inc., publishers.)

Previous Models

The intestinal model used in internal dosimetry calculations in the OLINDA/EXM software (116), and the preceding program MIRDOSE (115) is the MIRD model of the gastro-intestinal tract (103). The MIRD GI tract model considers the intestines as a possible excretion path but does not take into account the activity uptake in the intestinal wall. The model of the small intestine consists of a box with curved short sides.

In the model described by the International Commission on Radiation Protection (ICRP) (125) the specific absorbed fraction is calculated for the mucosal layer of the intestine for non-penetrating radiation. For penetrating radiation the small intestine is modelled as a large soft tissue volume where the wall and contents are not differentiated. The average absorbed dose to the wall and contents represents the absorbed dose to the mucosal layer.

The absorbed dose to the wall or mucus layer from photons is calculated as the average dose for wall and contents (103,126) and for electrons the absorbed dose to the wall is calculated as the surface dose, i.e. the dose to the wall is half the dose to the contents far from the wall (the “one-half-

assumption”)(103,125). The specific absorbed fraction, SAF, to the wall from non-penetrating radiation in the contents is given by:

$$SAF(\text{wall} \leftarrow \text{contents}) = \frac{1}{2M_{\text{contents}}} \cdot \nu \quad (24)$$

where M_{contents} is the mass of the intestinal contents and the factor ν represents the penetration of the radiation to the radiation-sensitive cells in the wall, and is taken to be 1 for electrons and 0.01 for α -particles (125).

The cylinder model of the small intestine was introduced by Poston et al. in 1996 (127). They described the small intestine as concentric cylinders divided into 100- μm -thick tissue layers, and calculated the absorbed fraction to these layers. Assuming that the radiation-sensitive cells were located at a certain depth in the small intestinal wall, the specific absorbed fractions were calculated for electrons of various energies for this part of the small intestinal wall with the source located in the intestinal contents.

In a study by Stubbs et al. (128) the small intestine was modelled in a similar way to that in the study by Poston et al. (127). Calculations of S values for both electrons and photons as a function of depth in the intestinal wall were made for ^{90}Y (electrons only), ^{123}I , ^{131}I and $^{99\text{m}}\text{Tc}$ with the radionuclides distributed in the small intestinal contents.

In a recent study by Bhuiyan and Poston (129), the absorbed dose was calculated as a function of depth in the intestinal wall in the cylinder model for a source of electrons uniformly distributed in the contents.

These studies have in common that only the intestinal contents is regarded as a source of the radionuclide. The intestinal wall or parts of it are not considered as source volumes in the models above.

Our Extended Model

In the studies on dosimetry for the small intestine (**Papers I and II**) the cylinder model was refined by calculating the absorbed dose for possible activity uptake in the intestinal wall as well as for excretion of the activity via the intestinal tract, i.e. source volumes were regarded as either the small intestinal wall or as the contents of the intestine. The cross-dose was also considered by modelling the intestinal loops as closely packed cylinders in a hexagonal arrangement (Fig. 8).

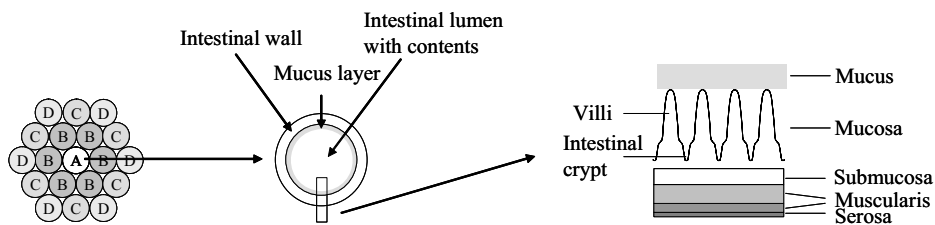


Figure 8. The geometrical model of the small intestine used in the present studies. The cross-dose model is shown on the left. The general cylinder model is shown in the centre and on the right the cross section of the intestinal wall is illustrated. (Reprinted by permission of the Society of Nuclear Medicine from (130).)

In the study presented in **Paper II**, the absorbed dose was calculated for an activity homogeneously distributed throughout the whole intestinal wall. The model can, however, be modified to address the activity uptake in one or several concentric rings in the cylinder model, i.e. different layers in the wall. For the absorbed dose calculations presented in **Papers I and II**, a uniform activity distribution was assumed since ^{99m}Tc -sestamibi is taken up by the muscular cells in the body. Fisher et al. (12,16,120) used a model similar to ours to calculate the absorbed dose to the mucosa and the total intestinal wall with the activity located only in the intestinal mucosa.

Four different values of the mucus thickness were used, 5, 50, 100 and 200 μm . The choice of mucus thickness affects the absorbed dose to the radiation-sensitive mucosal cells for electron sources located in the intestinal contents. In a study by Bhuiyan et al. (129) a model of the small intestine very similar to ours is used. Their study concerns absorbed dose calculations for several electron energies. For electron energies with CSDA ranges corresponding to the depth of the crypt cells, a change in mucus layer thickness can result in a variation in absorbed dose to the sensitive cells of several orders of magnitude (129). In the present work (**Paper I**), the electron energies were either lower or higher than electron CSDA ranges corresponding to the sensitive cell depth in the wall, and this variation is therefore not seen for the crypt cells in this investigation. However, the S values for the villi show a variation with mucus layer thickness for energies of 50 to 200 keV. With the activity located in the intestinal wall, the lumen radius has only a minor effect on the absorbed dose (16). The wall thickness can instead affect the calculated absorbed dose as the mass of the wall increases.

Importance of an Improved Small Intestinal Model

An observation made in several of the papers (112,127-129) is the overestimation of the absorbed dose to the mucosal layer when using the current dosimetry model. The assumption expressed in Eqn (24) overestimates the absorbed fraction in the sensitive cells of the small intestine by up to several orders of magnitude (128). Concerning electron sources located in the intestinal contents, the fraction of the energy absorbed in the sensitive cells is largely dependent on the electron energy and the depth of the cells. For energies below 100 keV the contribution to the sensitive cells is of minor importance (112,129). For electron energies of a few hundred keV and higher the absorbed fraction shows considerable variation with depth in the intestinal wall and Han et al. (112) suggest that for electron energies exceeding 100 keV the energy transport should be accounted for. For energies above 500 keV the absorbed fraction is not dependent on the depth in the wall (131) due to the long range of the electrons.

At electron energies below a few MeV the self-dose from the wall and from the contents is several orders of magnitude higher than the cross-dose. The self-dose from electrons in the intestinal wall also exceeds the self-dose from the contents for the energies studied in **Paper I**, and below about 200 keV by several orders of magnitude. This emphasizes the importance of improving our knowledge on the activity biodistribution and possible uptake in the intestinal wall or mucosa.

The model of the small intestine used in absorbed dose calculation programs today (115,116) uses the “one-half assumption” described above (Eqn 24). It is given as the absorbed dose to the contents-wall interface from the activity in the contents. This assumption overestimates the absorbed dose to the sensitive cells in the mucosa (112,128,129). This could be corrected for in Eqn 24 by using ν values, unique for each radionuclide, or for electrons, for a certain energy interval (128). Stubbs et al. (128) have suggested values of ν for some radionuclides, for example, 10^{-4} for radionuclides emitting low-energy conversion or Auger electrons, e.g. ^{99m}Tc , while for high-energy β -emitters such as ^{90}Y , Eqn 24 can still be used. These models only consider the contents as source location.

Most studies using a cylindrical model of the small intestine are based on similar data for the dimensions of the small intestine (Table 1). The ICRP has recently published a new model for the alimentary tract (132) for radiation protection purposes. In their compartment model absorption from the contents and retention of the radionuclides in the intestinal wall is also taken into account. A cylindrical model is adopted with an internal diameter of the

small intestine of 2 cm and the sensitive cell layer is assumed to be located 130-150 μm from the intercryptal plate at the base of the villi, in the case of a uniformly distributed radioactive source in the contents. This short distance between contents and sensitive cell layer is explained by the assumed penetration of the intestinal contents between the villi. In this model the intestinal wall is also a possible source with the radionuclide either located in the villi, which consist of a 500- μm -thick uniform layer above the intercryptal plate, or distributed in a 200- μm -thick layer of the mucosa beneath the villi.

Table 1. Data for various small intestinal dosimetry models

Reference	Inner radius (mm)	Wall thickness (mm)	Villi height (μm)	Crypt depth (μm)	Mucus thickness (μm)	Depth of sensitive cell layer (μm)
ICRP 30 (125)	10	2-3	500-1500	20 - 450	-	520-1950
MIRD (6)	-	3-4	-	-	-	-
Stubbs et al. (128)	10	5	500	150	200	700-850
Poston et al. (127)	12.46	7.54	-	-	-	300-600
Jönsson et al. (130)	12.5	3 and 6	500	150	5-200	505-850
Breitz et al. (120)	2.85	3.5	-	-	-	600
Bhuiyan et al. (129)	14	3	500	150	210	710-860
ICRP 100 (132)	10	-	500	-	-	130-150

*Mucosa thickness

The absorbed fractions for a number of electron energies, for sources in the small intestinal contents and in the villi, are published for the adult male in the report. Data for adult female and other age groups will be given in coming publications. Concerning the absorbed fraction for photons and radionuclides, it is planned to derive data using voxel-based phantoms which would be appropriate as reference anatomical models for radiation protection purposes.

Summary of Papers

Paper I: The development and refinement of a dosimetric cylinder model of the small intestine are presented. This model was used for Monte Carlo simulations of S values for the crypt cells in the mucosa as target organ. The EGS4 Monte Carlo simulation package with the PRESTA algorithm was used for the simulations. S values were calculated for the intestinal wall and the contents as source organs for both self-dose and cross-dose from surrounding parts of the small intestine. Calculations of S values for self-dose and cross-dose were made for monoenergetic electrons, 0.050-10 MeV, and for the radionuclides ^{99m}Tc , ^{111}In , ^{131}I , ^{67}Ga and ^{211}At . It was shown that the cross-dose can be higher than the self-dose to the crypt cells, depending on the radionuclide and the activity distribution in the contents and/or wall, and also that the mucus thickness affects the S value when the activity is located in the contents.

Paper II: Calculations of the absorbed dose to the crypt cells for a realistic activity distribution are presented and the results are compared with the commonly used MIRDOSE3 calculation program and with published data. The absorbed dose was calculated taking into consideration the biodistribution of the radiopharmaceutical in the small intestinal wall and its contents, based on data obtained in rats. Absorbed dose calculations were performed using the intestinal model developed in the previous study. A maximum of 6% of the injected activity was found to be located in the intestinal wall 30 minutes post injection and 13% in the intestinal contents after 2 h, resulting in an absorbed dose of $8.9 \mu\text{Gy MBq}^{-1}$ to the crypt cells. Assuming the activity to be located only in the wall, the absorbed dose to the crypt cells was found to be 2.5 times higher than if all the activity is assumed to be in the intestinal contents.

Using the new intestinal dosimetry model, together with detailed biokinetic data for the radiopharmaceutical from animal studies, it is possible to calculate the absorbed dose to the crypt cells, which is not possible when using external imaging. The calculated absorbed dose was comparable with the results of calculations performed with the MIRDOSE3 computer program using small intestinal contents as the only source tissue. This study illustrates the importance of detailed biodistribution data for radiopharmaceuticals excreted through the intestinal tract, (obtainable via animal studies) and of using a detailed dosimetry model for the crypt cells, considering both self-dose and cross-dose from the intestinal wall and contents.

Paper III: In this study planar ^{99m}Tc images were simulated and two methods of attenuation correction and scatter compensation were investigated. An effective attenuation coefficient (EAC) was used as a combination of attenuation correction and scatter compensation and this was compared with a scatter correction using the TEW method together with a transmission factor image (SC-TF) for attenuation correction pixel by pixel. Scintillation camera images were simulated using a realistic activity distribution obtained in an animal study. The problem of activity in overlapping organs is demonstrated for the kidneys using this particular biodistribution. Due to activity in muscles and excretion of activity via the intestines it is difficult to find parts of the kidneys not influenced by activity in other tissues. The variation in the activity surrounding the kidneys makes the selection of the area for background subtraction quite difficult.

To validate the simulation method and to compare the correction methods, organs were also simulated separately and the organ activity was quantified. To allow comparison with the clinical situation, the total activity distribution from the animal study was used to simulate scintillation camera images at different points in time, and the calculated activity was compared with both the input data and some patient data from the literature.

The combination of scatter and attenuation correction gave the most accurate calculated activity, $\pm 10\%$ of the true activity obtained from the images for separate organs. In the images similar to the clinical situation, the kidney activity was overestimated by up to a factor of 34, mainly due to the excretion of activity through the intestines.

A novel approach to generating simulated human images of radionuclide biodistribution is described. Using the animal biodistribution data for simulations of scintillation camera images provides an opportunity to compare simulated images with images obtained from a patient study. Input data can be adjusted to obtain better agreement between the patient image data and the simulated data. The input activity data used will thus give a more reliable activity distribution than the activities calculated from the patient images. Good agreement between activity data obtained from simulated images, from animal data, and patient images could be an indication of greater reliability of animal data in absorbed dose calculations for patients.

Paper IV: Planar scintillation camera images were simulated using the Zubal phantom and animal biodistribution data. The organ activity was determined through ROI analysis, using the conjugate-view method, and the SC-TF

methods were used for scatter and attenuation corrections. The residence times were calculated for the evaluated image activity data and for the animal biodistribution data. Phantom-specific S values were calculated and used for absorbed dose calculations, which were compared with absorbed doses calculated from the MIRDO-phantom-specific S values. Calculations were performed for both ^{99m}Tc and ^{131}I .

Overestimated organ activities in the kidneys due to overlapping tissues in the scintillation camera images resulted in 9.6 times higher residence time for ^{99m}Tc and 11.8 times higher for ^{131}I . The resulting absorbed dose for ^{131}I calculated with the Zubal S values was 6.9 times higher than the true absorbed dose. The corresponding result for the MIRDO S values was 10 times. Calculations for ^{99m}Tc were overestimated to a lower degree. The absorbed dose was less overestimated than the residence time because a significant fraction of the absorbed dose is given by the activity in surrounding tissues. The results also illustrate the potential inaccuracy of the calculated absorbed dose to a specific individual (in this case the Zubal phantom) when using the S values based on the MIRDO stylized phantom. The method used in this study was shown to be useful for evaluation of the accuracy of internal dosimetry.

Future Perspectives

In radionuclide therapy, the absorbed dose is calculated in order to predict the tumour response and possible side-effects on normal tissue. The accuracy of the calculated absorbed dose depends on the methods to quantify the activity in different organs and tissues in the body, and on the dosimetric model used.

Improvements are necessary in both the quantification procedure and in the development of new and more realistic, small-scale anatomy models. Using detailed data on the activity uptake in tissues and cells may allow the integration of models and patient-specific dosimetry.

The conjugate-view method for activity quantification from planar scintillation camera images that was investigated in this work only provides information about the activity distribution in two dimensions. Consequently, it is often difficult to compensate for activity in overlapping organs. The problems of attenuation and scatter are not fully corrected for. SPECT, on the other hand, has the potential to overcome many of the problems associated with planar imaging, and accurate compensation for scatter, attenuation and collimator response can be included in iterative reconstructions. The limitations of SPECT are the time required and the limited field of view of the images. A possible next step for a practical dosimetry protocol could therefore be the combination of planar images at several points in time to account for the biokinetics in different organs with one or more SPECT studies to scale this variation to the actual activity in the tissues (133).

It is important to distinguish between dosimetry for late-effect risk estimates and for dose planning for treatment with radionuclides. The phantoms included in programs such as OLINDA have been developed to reflect a reference human for dosimetry in diagnostic procedures. In radionuclide therapy the aim is to provide deterministic effects to malignant tissue as much as possible without causing harmful side effects on normal tissues. Patient-specific geometry is therefore more important in this case. The most accurate way of obtaining patient-specific geometry is to use a CT scan and the radionuclide distribution using multiple quantitative SPECT studies. The absorbed dose can then be simulated using the Monte Carlo method employing this information, to obtain absorbed dose distributions on a voxel-by-voxel level. The variation in absorbed doses within a particular organ can then be described as, for example, a dose-volume histogram (DVH) by segmentation of organ volumes from the CT images (134). The absorbed dose

distribution can be presented in the form of a DVH showing the fraction of the organ or tumour receiving a certain absorbed dose as a function of absorbed dose (differential DVH) or the fraction of the tissue receiving less than a specified dose versus the absorbed dose (integral DVH) (29,135).

The vision of using multiple SPECT/CT measurements for improved dosimetry is not too far away, due to the recent successful development of the hybrid SPECT/CT systems which are today commercially available. The major vendors of SPECT systems now offer very time-efficient systems including high-quality, fast CT acquisition providing accurate registration to the SPECT images.

In external radiation therapy, in principle, part of the patient's body is uniformly irradiated with photon or particle beams. The energy absorbed in a small tissue volume is then uniformly distributed within that volume, at least compared with the situation in nuclear medicine. For that reason, the absorbed dose in external radiation therapy can be accurately calculated from a physical point of view, and dose-effect relationships can be obtained, although many other factors may influence the biological effects.

One major problem in internal dosimetry calculations is the fact that the radiation source distribution is initially unknown. In external radiation therapy the radiation output from linear accelerators is very well defined and well-known and can be turned on and off. When administering radionuclides these continue to emit radiation with a certain half-life, and the distribution changes with time. The imaging system used to determine the *in vivo* distribution has known limitations in spatial resolution, and the errors associated with internal dosimetry depend largely on the way the radionuclide distribution is measured. The imaging systems used for internal dosimetry today can give a reliable time-activity distribution, and absorbed dose rates at voxel level can be obtained from the tomography studies.

Even if a perfectly accurate scatter and attenuation correction method could be developed for SPECT, activity distributions in volumes smaller than the spatial resolution of the system could not be achieved. A connection to a small-scale model for the particular tissue and radiopharmaceutical will probably be necessary. For example, the dosimetry and the biological effects on a tumour are influenced by several factors, such as the type and energy of emitted radiation, the distance to the cell target, the size of the tumour and the activity uptake. Considerable effort is being made in this area to calculate absorbed fractions, S values and tumour-to-normal-tissue mean absorbed dose-rate ratios for different dosimetric models and radionuclides (136-141).

The value of the absorbed dose is in itself of no interest unless it can be related to some kind of biological effect. According to Sgouros (20), only a few studies have demonstrated a dose-effect relationship, while most have failed to show a relation, mainly due to biological factors and differences in dosimetry methodologies. This lack of relationship is partly due to the use of the mean absorbed dose. The distribution of a radiopharmaceutical is rarely uniform within an organ and the absorbed dose to different cells in the organ will vary. Several studies have shown this heterogeneity in for example, the kidneys, intestines, liver, spleen, lungs and testes. (124,142,143). (More studies have been reviewed in the ICRU report No 67 (142)). There is therefore a need for detailed information concerning the activity distribution within the organs down to the cell level in order to be able to improve internal dosimetry and make reliable absorbed dose calculations. For example, Bolch et al. (144) are working on a new 3D skeletal and bone marrow model obtained from human data, where they also include the microscopic structure of the bone matrix to better calculate absorbed fractions from particles emitted in the bone marrow or from the bone surfaces. The simple assumption of a mean absorbed dose has proven to be inaccurate, especially for high electron energies, where a more accurate bone structure obtained from micro-CT studies has proven to make a difference.

Since it is usually difficult to achieve detailed biological data from patient imaging studies, detailed animal data can be very helpful and provide an important tool in obtaining more realistic models for dosimetric calculations. As suggested in **Paper III**, images of an activity biodistribution can be simulated and compared with patient images. By adjusting the input data and performing new simulations that produce new scintillation camera images the procedure can be repeated until the image is as close to the patient image as possible. The input data for the simulation is then representing a probable activity distribution in the patient.

It was shown in **Papers III and IV** that this method can be useful for the evaluation of the accuracy of quantification, correction and calculation methods in internal dosimetry. As Zanzonico pointed out in an invited commentary, (145) our work on the small-scale anatomic model of the small intestine (**Paper I**) in combination with detailed data on the activity uptake in organs or cells, is one way of integrating model-based and patient-specific dosimetry.

Regarding the intestinal model developed in this work a further improvement could be achieved by using the NCAT computer phantom (57) of the thorax and abdomen. This phantom is based on non-uniform rational B-splines (NURBS) to define the surfaces of individual organs. These surfaces can then be adjusted. The program provides images and any matrix resolution can be used as input to Monte Carlo programs like those used in this thesis. The advantages of a phantom like NCAT are that it provides a more realistic geometry than the earlier MIRD phantoms, and that the size and locations of the organs can be modified. A recent modification of the NCAT phantom allows the intestinal wall to be defined. Activity can be located in the intestinal wall and the transport of activity in the contents can be simulated. Scintillation camera images can be simulated and compared with clinical images.

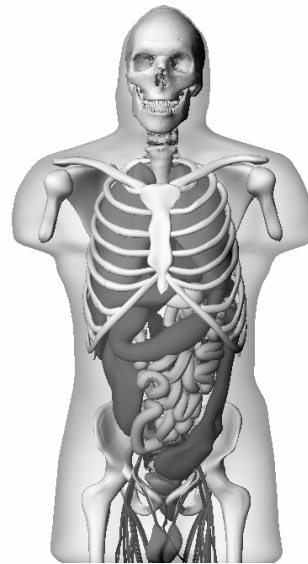


Figure 9. The NCAT computer phantom. *(Reprinted by permission of Dr. Segars Duke University, North Carolina.)*

Acknowledgements

During the course of the work described in this thesis several people have helped and supported me in many ways. I would particularly like to express my appreciation to the following:

My supervisor, Professor *Sven-Erik Strand*, for introducing me to the field of nuclear medicine for his guidance, support, never-ending optimism and continuous friendship during many years;

My supervisor, Professor *Michael Ljungberg*, for his trust and generous support and friendship. Thank you for always keeping your door and your Skype connection open for discussion;

Carin Lingårdh and *Karin Wingårdh*, for technical assistance and support during my work and for our discussions about most everything;

Cecilia Hindorf, *Katarina Sjögren-Gleisner* and *Ronnie Wirestam* for their inspiration and valuable scientific and not so scientific discussions;

All former and present friends and colleagues at the Department of Medical Radiation Physics in Lund for pleasant company and friendship and for help in many different ways;

Friends and colleagues at the Department of Radiation Physics, Lund University Hospital and Malmö University Hospital, the Department of Medical Radiation Physics, Malmö and BFC Clinical Physiology at Lund University Hospital;

Helen Sheppard, for professionally correcting the manuscripts;

Friends outside the department for their help and encouragement during the years;

Special thanks to my family, especially my dear husband and collaborator *Bo-Anders*, who has continuously supported me especially during the completion of this thesis. My dear, dear children, *Maria* and *Fredrik* for their love and patience, for bringing me down to earth and putting things into perspective.

This work was generously supported by The Swedish Cancer Foundation, The Gunnar Nilsson Foundation, The Swedish Medical Research Council, Lund University Hospital Donation Funds, Berta Kamprad's Foundation and John and Augusta Persson's Foundation for Medical Research.

References

- (1) The Swedish Radiation Protection Authority SSI. Isotope statistics in nuclear medicine (Isotopkommittérapporter). 2007. www.ssi.se.
- (2) Wiseman GA, White CA, Sparks RB et al. Biodistribution and dosimetry results from a phase III prospectively randomized controlled trial of Zevalin radioimmunotherapy for low-grade, follicular, or transformed B-cell non-Hodgkin's lymphoma. *Crit Rev Oncol Hematol*. 2001;39(1-2):181-194.
- (3) Vose JM. Bexxar: novel radioimmunotherapy for the treatment of low-grade and transformed low-grade non-Hodgkin's lymphoma. *Oncologist*. 2004;9(2):160-172.
- (4) Macklis RM. Iodine-131 tositumomab (Bexxar) in a radiation oncology environment. *Int J Radiat Oncol Biol Phys*. 2006;66(2 Suppl):S30-S34.
- (5) Meredith RF. Ongoing investigations and new uses of radioimmunotherapy in the treatment of non-Hodgkin's lymphoma. *Int J Radiat Oncol Biol Phys*. 2006;66(2 Suppl):S23-S29.
- (6) Snyder WS, Ford MR, Warner GG. Estimates of specific absorbed fractions for photons sources uniformly distributed in various organs of a heterogeneous phantom. 1978. MIRD Pamphlet No. 5 (revised). New York, NY: Society of Nuclear Medicine.
- (7) Statens strålskyddsinstitut. Statens strålskyddsinstituts föreskrifter och allmänna råd om nukleärmedicin. SSI FS 2000:3. 2000. www.ssi.se.
- (8) Council directive 97/43/Euratom. On health protection of individuals against the dangers of ionizing radiation in relation to medical exposure, and repealing Directive 84/466/Euratom. 1997.
- (9) Gopal AK, Gooley TA, Maloney DG et al. High-dose radioimmunotherapy versus conventional high-dose therapy and autologous hematopoietic stem cell transplantation for relapsed follicular non-Hodgkin lymphoma: a multivariable cohort analysis. *Blood*. 2003;102(7):2351-2357.
- (10) Breitz H. Clinical aspects of radiation nephropathy. *Cancer Biother Radiopharm*. 2004;19(3):359-362.
- (11) Moll S, Nickleit V, Mueller-Brand J, Brunner FP, Maecke HR, Mihatsch MJ. A new cause of renal thrombotic microangiopathy: yttrium 90-DOTATOC internal radiotherapy. *Am J Kidney Dis*. 2001;37(4):847-851.
- (12) Knox SJ, Goris ML, Tempero M et al. Phase II trial of yttrium-90-DOTA-biotin pretargeted by NR-LU-10 antibody/streptavidin in patients with metastatic colon cancer. *Clin Cancer Res*. 2000;6(2):406-414.

- (13) Giralt S, Bensinger W, Goodman M et al. 166Ho-DOTMP plus melphalan followed by peripheral blood stem cell transplantation in patients with multiple myeloma: results of two phase 1/2 trials. *Blood*. 2003;102(7):2684-2691.
- (14) Sgouros G, Stabin M, Erdi Y et al. Red marrow dosimetry for radiolabeled antibodies that bind to marrow, bone, or blood components. *Med Phys*. 2000;27(9):2150-2164.
- (15) Fisher DR. Assessments for high dose radionuclide therapy treatment planning. *Radiat Prot Dosimetry*. 2003;105(1-4):581-586.
- (16) Fisher D, Rajon D, Breitz H, Goris M, Bolch W, Knox S. Dosimetry model for radioactivity localized to intestinal mucosa. *Cancer Biother Radiopharm*. 2004;19(3):293-307.
- (17) Koral KF, Dewaraja Y, Clarke LA et al. Tumor-absorbed-dose estimates versus response in tositumomab therapy of previously untreated patients with follicular non-Hodgkin's lymphoma: preliminary report. *Cancer Biother Radiopharm*. 2000;15(4):347-355.
- (18) Wong JY, Wang J, Liu A et al. Evaluating changes in stable chromosomal translocation frequency in patients receiving radioimmunotherapy. *Int J Radiat Oncol Biol Phys*. 2000;46(3):599-607.
- (19) DeNardo GL, Juweid ME, White CA, Wiseman GA, DeNardo SJ. Role of radiation dosimetry in radioimmunotherapy planning and treatment dosing. *Crit Rev Oncol Hematol*. 2001;39(1-2):203-218.
- (20) Sgouros G. Dosimetry of internal emitters. *J Nucl Med*. 2005;46 Suppl 1:18S-27S.
- (21) Flux G, Bardies M, Monsieurs M, Savolainen S, Strands SE, Lassmann M. The impact of PET and SPECT on dosimetry for targeted radionuclide therapy. *Z Med Phys*. 2006;16(1):47-59.
- (22) Forssell-Aronsson E, Kjellen E, Mattsson S, Hellstrom M. Medical imaging for improved tumour characterization, delineation and treatment verification. *Acta Oncol*. 2002;41(7-8):604-614.
- (23) Sorenson J. Methods for quantitation of radioactivity *in vivo* by external counting measurements. Ph.D.Thesis . 1971. University of Wisconsin, Madison, Wisconsin.
- (24) Thomas SR, Maxon HR, Kereiakes JG, Saenger EL. Quantitative external counting techniques enabling improved diagnostic and therapeutic decisions in patients with well-differentiated thyroid cancer. *Radiology*. 1977;122(3):731-737.
- (25) Fleming JS. A technique for the absolute measurement of activity using a gamma camera and computer. *Phys Med Biol*. 1979;24(1):176-180.
- (26) Kojima A, Ohyama Y, Tomiguchi S et al. Quantitative planar imaging method for measurement of renal activity by using a conjugate-emission image and transmission data. *Med Phys*. 2000;27(3):608-615.

- (27) Kemerink GJ, Liem IH, Hofstra L et al. Patient dosimetry of intravenously administered ^{99m}Tc -annexin V. *J Nucl Med.* 2001;42(2):382-387.
- (28) Loevinger R, Budinger T, Watson E. MIRD primer for absorbed dose calculations. 1988. Society of Nuclear Medicine, New York, NY.
- (29) Zanzonico PB. Internal radionuclide radiation dosimetry: a review of basic concepts and recent developments. *J Nucl Med.* 2000;41(2):297-308.
- (30) Fisher DR. Internal dosimetry for systemic radiation therapy. *Semin Radiat Oncol.* 2000;10(2):123-132.
- (31) Stabin MG. Developments in the internal dosimetry of radiopharmaceuticals. *Radiat Prot Dosimetry.* 2003;105(1-4):575-580.
- (32) Song H, He B, Prideaux A et al. Lung Dosimetry for Radioiodine Treatment Planning in the Case of Diffuse Lung Metastases. *J Nucl Med.* 2006;47(12):1985-1994.
- (33) Kontogeorgakos DK, Dimitriou PA, Limouris GS, Vlahos LJ. Patient-specific dosimetry calculations using mathematic models of different anatomic sizes during therapy with ^{111}In -DTPA-D-Phe 1 -octreotide infusions after catheterization of the hepatic artery. *J Nucl Med.* 2006;47(9):1476-1482.
- (34) Gardin I, Linhart NC, Petiet A, Bok B. Dosimetry at the cellular level of Kupffer cells after technetium- 99m -sulphur colloid injection. *J Nucl Med.* 1992;33(3):380-384.
- (35) Makrigiorgos GM, Adelstein SJ, Kassis AI. Cellular radiation dosimetry and its implications for estimation of radiation risks. Illustrative results with technetium 99m -labeled microspheres and macroaggregates. *JAMA.* 1990;264(5):592-595.
- (36) Andreo P. Monte Carlo techniques in medical radiation physics. *Phys Med Biol.* 1991;36(7):861-920.
- (37) Zaidi H. Relevance of accurate Monte Carlo modeling in nuclear medical imaging. *Med Phys.* 1999;26(4):574-608.
- (38) Ljungberg M, Strand S-E. A Monte Carlo Program Simulating Scintillation Camera Imaging. *Comp Meth Progr Biomed.* 1989;29:257-272.
- (39) Lewellen TK, Anson CP, Haynor DR et al. Design of a simulation system for emission tomographs. *J Nucl Med.* 1988;29(5):871.
- (40) Lewellen TK, Harrison RL, Vannoy S. The SIMSET program. In: Ljungberg M, Strand S-E, King MA, eds. *Monte Carlo calculations in nuclear medicine. Applications in diagnostic imaging.* Bristol and Philadelphia: IOP Publishing; 1998.
- (41) Gustafsson A, Arlig A, Jacobsson L, Ljungberg M, Wikkelso C. Dual-window scatter correction and energy window setting in cerebral blood flow SPECT: a Monte Carlo study. *Phys Med Biol.* 2000;45(11):3431-3440.

- (42) Arlig A, Gustafsson A, Jacobsson L, Ljungberg M, Wikkelso C. Attenuation correction in quantitative SPECT of cerebral blood flow: a Monte Carlo study. *Phys Med Biol.* 2000;45(12):3847-3859.
- (43) King MA, Xia W, deVries DJ et al. A Monte Carlo investigation of artifacts caused by liver uptake in single-photon emission computed tomography perfusion imaging with technetium 99m-labeled agents. *J Nucl Cardiol.* 1996;3(1):18-29.
- (44) King MA, deVries DJ, Pan TS, Pretorius PH, Case JA. An investigation of the filtering of TEW scatter estimates used to compensate for scatter with ordered subset reconstructions. *IEEE Trans Nucl Sci.* 1997;44(3):1140-1145.
- (45) Berger MJ, Selzer SM. Electron and photon transport programs: I. Introduction and notes on program DATAPAC 4; II. Notes on program ETRAN. Reports NBS 9836 and 9837. 1968. Gaithersburg, MD, National Bureau of Standards.
- (46) RSIC. ETRAN: Monte Carlo code system for electron and photon transport through extended media. Report ORNL-RSIC CCC-107. 1968.
- (47) Nelson RF, Hirayama H, Rogers DWO. The EGS4 code system. SLAC 265. 1985. Stanford CA:SLAC.
- (48) Los Alamos National Laboratory: MCNP homepage. Online document at:<http://mcnp-green.lanl.gov/index.html>. 2007.
- (49) Buvat I, Lazaro D. Monte Carlo simulations in emission tomography and GATE: An overview. *Nucl Inst Meth in Phys Res.* 2006;569:323-329.
- (50) Santin G, Strul D, Lazaro D et al. GATE: A Geant4-based simulation platform for PET and SPECT integrating movement and time management. *IEEE Trans Nucl Sci.* 2003;50(5):1516-1521.
- (51) Zubal IG, Harrell CR, Smith EO, Rattner Z, Gindi G, Hoffer PB. Computerized three-dimensional segmented human anatomy. *Med Phys.* 1994;21(2):299-302.
- (52) Clairand I, Bouchet LG, Ricard M, Durigon M, Di PM, Aubert B. Improvement of internal dose calculations using mathematical models of different adult heights. *Phys Med Biol.* 2000;45(10):2771-2785.
- (53) Petoussi-Henss N, Zanki M, Fill U, Regulla D. The GSF family of voxel phantoms. *Phys Med Biol.* 2002;47(1):89-106.
- (54) Zankl M, Petoussi-Henss N, Fill U, Regulla D. The application of voxel phantoms to the internal dosimetry of radionuclides. *Radiat Prot Dosimetry.* 2003;105(1-4):539-548.
- (55) Caon M. Voxel-based computational models of real human anatomy: a review. *Radiat Environ Biophys.* 2004;42(4):229-235.
- (56) Segars WP, Lalush DS, Tsui BMW. A realistic spline-based dynamic heart phantom. *IEEE Trans Nucl Sci.* 1999;46(3pt2):503-506.

- (57) Segars WP, Lalush DS, Tsui BMW. Modelling respiratory mechanics in the MCAT and spline-based MCAT phantoms. *IEEE Trans Nucl Sci.* 2001;48(1pt1):89-97.
- (58) Siegel JA, Thomas SR, Stubbs JB et al. MIRDO pamphlet no. 16: Techniques for quantitative radiopharmaceutical biodistribution data acquisition and analysis for use in human radiation dose estimates. *J Nucl Med.* 1999;40(2):37S-61S.
- (59) Jönsson BA, Strand SE, Andersson L. Radiation dosimetry for indium-111-labeled anti-CEA-F(ab)² fragments evaluated from tissue distribution in rats. *J Nucl Med.* 1992;33(9):1654-1660.
- (60) Dewaraja YK, Ljungberg M, Koral KF. Characterization of scatter and penetration using Monte Carlo simulation in 131I imaging. *J Nucl Med.* 2000;41(1):123-130.
- (61) Sjögreen K, Ljungberg M, Strand SE. An activity quantification method based on registration of CT and whole-body scintillation camera images, with application to 131I. *J Nucl Med.* 2002;43(7):972-982.
- (62) Minarik D, Sjögreen K, Ljungberg M. A new method to obtain transmission images for planar whole-body activity quantification. *Cancer Biother Radiopharm.* 2005;20(1):72-76.
- (63) Delpon G, Ferrer L, Lenta C, Lisbona A, Buvat I, Bardies M. Comparison of four scatter correction methods for patient whole-body imaging during therapeutic trials with iodine-131. *Cancer.* 2002;94(4 Suppl):1224-1230.
- (64) Hammond ND, Moldofsky PJ, Beardsley MR, Mulhern CB, Jr. External imaging techniques for quantitation of distribution of I-131 F(ab)² fragments of monoclonal antibody in humans. *Med Phys.* 1984;11(6):778-783.
- (65) Green AJ, Dewhurst SE, Begent RH, Bagshawe KD, Riggs SJ. Accurate quantification of 131I distribution by gamma camera imaging. *Eur J Nucl Med.* 1990;16(4-6):361-365.
- (66) Shen S, DeNardo GL, DeNardo SJ. Quantitative bremsstrahlung imaging of yttrium-90 using a Wiener filter. *Med Phys.* 1994;21(9):1409-1417.
- (67) DeNardo GL, Shen S, DeNardo SJ et al. Quantification of iodine-131 in tumors using a threshold based on image contrast. *Eur J Nucl Med.* 1998;25(5):497-502.
- (68) Zaidi H, Hasegawa B. Determination of the attenuation map in emission tomography. *J Nucl Med.* 2003;44(2):291-315.
- (69) Bloch P, Sanders T. Reduction of the effects of scattered radiation on a sodium iodide imaging system. *J Nucl Med.* 1973;14:67-72.
- (70) van Reenen PC, Lotter MG, Heyns AD et al. Quantification of the distribution of 111In-labelled platelets in organs. *Eur J Nucl Med.* 1982;7(2):80-84.
- (71) King MA, Hademenos GJ, Glick SJ. A dual-photopeak window method for scatter correction. *J Nucl Med.* 1992;33(4):605-612.

- (72) Pretorius PH, van Rensburg AJ, van AA, Lotter MG, Serfontein DE, Herbst CP. The channel ratio method of scatter correction for radionuclide image quantitation. *J Nucl Med.* 1993;34(2):330-335.
- (73) Jaszczak RJ, Greer KL, Floyd CE, Jr., Harris CC, Coleman RE. Improved SPECT quantification using compensation for scattered photons. *J Nucl Med.* 1984;25(8):893-900.
- (74) Koral KF, Clinthorne NH, Rogers WL. Improving Emission Computed Tomography Quantification by Compton Scatter Rejection through Offset Windows. *Nucl Inst Meth in Phys Res.* 1986;A242:610-614.
- (75) Thomas SR, Maxon HR, Kerciakes JG. In vivo quantitation of lesion radioactivity using external counting methods. *Med Phys.* 1976;3:253-255.
- (76) Jaszczak RJ, Coleman RE, Whitehead FR. Physical Factors affecting Quantitative Measurements using Camera-Based Single Photon Emission Computed Tomography (SPECT). *IEEE Trans Nucl Sci.* 1981;NS-28:69-80.
- (77) Macey DJ, Marshall R. Absolute quantitation of radiotracer uptake in the lungs using a gamma camera. *J Nucl Med.* 1982;23(8):731-734.
- (78) Ferrant A, Cauwe F. Quantitative organ-uptake measurement with a gamma camera. *Eur J Nucl Med.* 1979;4(3):223-229.
- (79) Wu RK, Siegel JA. Absolute quantitation of radioactivity using the buildup factor. *Med Phys.* 1984;11(2):189-192.
- (80) Siegel JA, Maurer AH, Wu RK et al. Absolute left ventricular volume by an iterative build-up factor analysis of gated radionuclide images. *Radiology.* 1984;151(2):477-481.
- (81) Siegel JA, Wu RK, Maurer AH. The buildup factor: effect of scatter on absolute volume determination. *J Nucl Med.* 1985;26(4):390-394.
- (82) van Rensburg AJ, Lotter MG, Heyns AD, Minnaar PC. An evaluation of four methods of ¹¹¹In planar image quantification. *Med Phys.* 1988;15(6):853-861.
- (83) Kojima A, Takaki Y, Matsumoto M et al. A preliminary phantom study on a proposed model for quantification of renal planar scintigraphy. *Med Phys.* 1993;20(1):33-37.
- (84) Ljungberg M, Strand SE. Attenuation correction in SPECT based on transmission studies and Monte Carlo simulations of build-up functions. *J Nucl Med.* 1990;31(4):493-500.
- (85) Yanch JC, Flower MA, Webb S. A comparison of deconvolution and windowed subtraction techniques for scatter compensation in SPECT. *IEEE transactions on medical imaging.* 1988;7(1):13-20.

- (86) Axelsson B, Msaki P, Israelsson A. Subtraction of Compton-scattered photons in single-photon emission computerized tomography. *J Nucl Med.* 1984;25(4):490-494.
- (87) Msaki P, Axelsson B, Larsson SA. Some physical factors influencing the accuracy of convolution scatter correction in SPECT. *Phys Med Biol.* 1989;34(3):283-298.
- (88) Hamill JJ, DeVito RP. Scatter reduction in energy-weighted acquisition. *IEEE Trans Nucl Sci.* 1989;36:1334-1339.
- (89) Halama JR, Henkin RE, Friend LE. Gamma camera radionuclide images: improved contrast with energy-weighted acquisition. *Radiology.* 1988;169(2):533-538.
- (90) DeVito RP, Hamill JJ, Treffert JD, Stoub EW. Energy-weighted acquisition of scintigraphic images using finite spatial filters. *J Nucl Med.* 1989;30(12):2029-2035.
- (91) Harris CC, Greer KL, Jaszczak RJ, Floyd CE, Jr., Fearnow EC, Coleman RE. Tc-99m attenuation coefficients in water-filled phantoms determined with gamma cameras. *Med Phys.* 1984;11(5):681-685.
- (92) Vestergren E, Jacobsson L, Mattsson S et al. Biokinetics and dosimetry of Tc-99m HM-PAO in children. oak ridge , 444-456. 1-1-1991.
- (93) Starck SA, Carlsson S. The determination of the effective attenuation coefficient from effective organ depth and modulation transfer function in gamma camera imaging. *Phys Med Biol.* 1997;42(10):1957-1964.
- (94) Buvat I, Benali H, Todd-Pokropek A, Di PR. Scatter correction in scintigraphy: the state of the art. *Eur J Nucl Med.* 1994;21(7):675-694.
- (95) Ogawa K, Harata Y, Ichihara T, Kubo A, Hashimoto S. A practical method for position-dependent compton-scatter correction in single photon emission CT. *IEEE transactions on medical imaging.* 1991;10(3):408-412.
- (96) Macey DJ, Grant EJ, Bayouth JE et al. Improved conjugate view quantitation of I-131 by subtraction of scatter and septal penetration events with a triple energy window method. *Med Phys.* 1995;22(10):1637-1643.
- (97) Buvat I, Rodriguez-Villafuerte M, Todd-Pokropek A, Benali H, Di PR. Comparative assessment of nine scatter correction methods based on spectral analysis using Monte Carlo simulations. *J Nucl Med.* 1995;36(8):1476-1488.
- (98) Krak NC, Boellaard R, Hoekstra OS, Twisk JW, Hoekstra CJ, Lammertsma AA. Effects of ROI definition and reconstruction method on quantitative outcome and applicability in a response monitoring trial. *Eur J Nucl Med Mol Imaging.* 2005;32(3):294-301.
- (99) Mortelmans L, Nuyts J, Van PG, Van dM, V, De RM, Suetens P. A new thresholding method for volume determination by SPECT. *Eur J Nucl Med.* 1986;12(5-6):284-290.

- (100) Erdi YE, Wessels BW, Loew MH, Erdi AK. Threshold estimation in single photon emission computed tomography and planar imaging for clinical radioimmunotherapy. *Cancer Res.* 1995;55(23 Suppl):5823s-5826s.
- (101) Dewaraja Y, Ljungberg M, Fessler J. Anatomical information based partial volume compensation for I-131 SPECT imaging in radioimmunotherapy. *J Nucl Med.* 2006;47:115P.
- (102) Buijs WC, Siegel JA, Boerman OC, Corstens FH. Absolute organ activity estimated by five different methods of background correction. *J Nucl Med.* 1998;39(12):2167-2172.
- (103) Snyder WS, Ford MR, Warner GG, Watson SB. "S", absorbed dose per unit cumulated activity for selected radionuclides and organs. MIRD Pamphlet No. 11. 1975. The Society of Nuclear Medicine, New York.
- (104) Cristy M, Eckerman K. Specific absorbed fractions of energy at various ages from internal photon sources. ORNL/TM-8381 V1-V7 (Oak Ridge, T: Oak Ridge National Laboratory) . 1987.
- (105) Stabin MG, Watson EE, Cristy M et al. Mathematical models and specific absorbed fractions of photon energy in the nonpregnant adult female and at the end of each trimester of pregnancy. ORNL/TM-12907. 1995. Oak Ridge National Laboratory, Oak Ridge, Tennessee, USA.
- (106) Coffey JL, Cristy M, Warner GG. Specific absorbed fractions for photon sources uniformly distributed in the heart chambers and heart wall of a heterogeneous phantom. *J Nucl Med.* 1981;22(1):65-71.
- (107) Thomas SR, Stabin MG, Chen CT, Samaratunga RC. MIRD Pamphlet No. 14 revised: A dynamic urinary bladder model for radiation dose calculations. Task Group of the MIRD Committee, Society of Nuclear Medicine. *J Nucl Med.* 1999;40(4):102S-123S.
- (108) Bouchet LG, Bolch WE, Weber DA, Atkins HL, Poston JW, Sr. MIRD Pamphlet No. 15: Radionuclide S values in a revised dosimetric model of the adult head and brain. Medical Internal Radiation Dose. *J Nucl Med.* 1999;40(3):62S-101S.
- (109) Bouchet LG, Bolch WE, Blanco HP et al. MIRD Pamphlet No 19: absorbed fractions and radionuclide S values for six age-dependent multiregion models of the kidney. *J Nucl Med.* 2003;44(7):1113-1147.
- (110) Bolch WE, Bouchet LG, Robertson JS et al. MIRD pamphlet No. 17: the dosimetry of nonuniform activity distributions--radionuclide S values at the voxel level. Medical Internal Radiation Dose Committee. *J Nucl Med.* 1999;40(1):11S-36S.
- (111) Stabin M. Nuclear medicine dosimetry. *Phys Med Biol.* 2006;51(13):R187-R202.
- (112) Han EY, Bolch WE, Eckerman KF. Revisions to the ORNL series of adult and pediatric computational phantoms for use with the MIRD schema. *Health Phys.* 2006;90(4):337-356.

- (113) ICRP International Commission on Radiological Protection. Basic anatomical and physiological data for use in radiological protection: reference values. ICRP publication 89. 2003. *Annals of the ICRP* 32 (3-4).
- (114) ICRU International Commission on Radiation Units and Measurements. Photon, electron, proton and neutron interaction data for body tissues. ICRU report 46. 1992. Bethesda, MD.
- (115) Stabin MG. MIRDOSE: personal computer software for internal dose assessment in nuclear medicine. *J Nucl Med.* 1996;37(3):538-546.
- (116) Stabin MG, Sparks RB, Crowe E. OLINDA/EXM: the second-generation personal computer software for internal dose assessment in nuclear medicine. *J Nucl Med.* 2005;46(6):1023-1027.
- (117) Watson EE, Stabin MG, Davis JL, Eckerman KF. A model of the peritoneal cavity for use in internal dosimetry. *J Nucl Med.* 1989;30(12):2002-2011.
- (118) Stabin MG. A model of the prostate gland for use in internal dosimetry. *J Nucl Med.* 1994;35(3):516-520.
- (119) Stabin MG, Yoriyaz H. Photon specific absorbed fractions calculated in the trunk of an adult male voxel-based phantom. *Health Phys.* 2002;82(1):21-44.
- (120) Breitz HB, Fisher DR, Goris ML et al. Radiation absorbed dose estimation for ⁹⁰Y-DOTA-biotin with pretargeted NR-LU-10/streptavidin. *Cancer Biother Radiopharm.* 1999;14(5):381-395.
- (121) Watanabe T, Terui S, Itoh K et al. Phase I study of radioimmunotherapy with an anti-CD20 murine radioimmunoconjugate ((⁹⁰Y-ibritumomab tiuxetan) in relapsed or refractory indolent B-cell lymphoma. *Cancer Sci.* 2005;96(12):903-910.
- (122) Henriksen G, Fisher DR, Roeske JC, Bruland OS, Larsen RH. Targeting of osseous sites with alpha-emitting ²²³Ra: comparison with the beta-emitter ⁸⁹Sr in mice. *J Nucl Med.* 2003;44(2):252-259.
- (123) Nilsson S, Larsen RH, Fossa SD et al. First clinical experience with alpha-emitting radium-223 in the treatment of skeletal metastases. *Clin Cancer Res.* 2005;11(12):4451-4459.
- (124) Jönsson BA, Strand SE, Larsson BS. A quantitative autoradiographic study of the heterogeneous activity distribution of different indium-111-labeled radiopharmaceuticals in rat tissues. *J Nucl Med.* 1992;33(10):1825-1833.
- (125) ICRP International Commission on Radiological Protection. Limits for intakes of radionuclides by workers. ICRP publication 30, part 1. 1979. *Annals of the ICRP* 2, (3-4).
- (126) ICRP International Commission on Radiological Protection. Report of the task group on reference man. ICRP publication 23. 1975. Pergamon Press, Oxford.

- (127) Poston JW, Jr., Kodimer KA, Bolch WE, Poston JW, Sr. A revised model for the calculation of absorbed energy in the gastrointestinal tract. *Health Phys.* 1996;71(3):307-314.
- (128) Stubbs JB, Evans JF, Stabin MG. Radiation absorbed doses to the walls of hollow organs. *J Nucl Med.* 1998;39(11):1989-1995.
- (129) Bhuiyan NU, Poston JW, Sr. A revised model for electron dosimetry in the human small intestine. *Health Phys.* 2005;88(1):23-36.
- (130) Jönsson L, Liu X, Jonsson BA, Ljungberg M, Strand SE. A dosimetry model for the small intestine incorporating intestinal wall activity and cross-doses. *J Nucl Med.* 2002;43(12):1657-1664.
- (131) Metivier H. A new model for the human alimentary tract: the work of a Committee 2 task group. *Radiat Prot Dosimetry.* 2003;105(1-4):43-48.
- (132) ICRP International Commission on Radiological Protection. Human alimentary tract model for radiological protection. ICRP publication 100. 2006. Annals of the ICRP vol 36 (1-2).
- (133) Koral KF, Dewaraja Y, Li J et al. Initial results for Hybrid SPECT--conjugate-view tumor dosimetry in ¹³¹I-anti-B1 antibody therapy of previously untreated patients with lymphoma. *J Nucl Med.* 2000;41(9):1579-1586.
- (134) ICRU International Commission on Radiation Units and Measurements. Absorbed-dose specification in nuclear medicine. ICRU report No 67. 2002. Ashford, Kent, England, Nuclear Technology Publishing.
- (135) Kolbert KS, Sgouros G, Scott AM et al. Implementation and evaluation of patient-specific three-dimensional internal dosimetry. *J Nucl Med.* 1997;38(2):301-308.
- (136) Siegel JA, Stabin MG. Absorbed fractions for electrons and beta particles in spheres of various sizes. *J Nucl Med.* 1994;35(1):152-156.
- (137) Bardies M, Chatal JF. Absorbed doses for internal radiotherapy from 22 beta-emitting radionuclides: beta dosimetry of small spheres. *Phys Med Biol.* 1994;39(6):961-981.
- (138) Bernhardt P, Forssell-Aronsson E, Jacobsson L, Skarnemark G. Low-energy electron emitters for targeted radiotherapy of small tumours. *Acta Oncol.* 2001;40(5):602-608.
- (139) Uusijärvi H, Bernhardt P, Ericsson T, Forssell-Aronsson E. Dosimetric characterization of radionuclides for systemic tumor therapy: influence of particle range, photon emission, and subcellular distribution. *Med Phys.* 2006;33(9):3260-3269.
- (140) Neti PV, Howell RW. Isolating effects of microscopic nonuniform distributions of ¹³¹I on labeled and unlabeled cells. *J Nucl Med.* 2004;45(6):1050-1058.

- (141) Hindorf C, Emfietzoglou D, Linden O, Kostarelos K, Strand SE. Internal microdosimetry for single cells in radioimmunotherapy of B-cell lymphoma. *Cancer Biother Radiopharm.* 2005;20(2):224-230.
- (142) ICRU International Commission on Radiation Units and Measurements. Absorbed-dose specification in nuclear medicine. ICRU report No 67. 2002. Ashford, Kent, England, Nuclear Technology Publishing.
- (143) Melis M, Krenning EP, Bernard BF, Barone R, Visser TJ, de JM. Localisation and mechanism of renal retention of radiolabelled somatostatin analogues. *Eur J Nucl Med Mol Imaging.* 2005;32(10):1136-1143.
- (144) Bolch WE, Patton PW, Rajon DA, Shah AP, Jokisch DW, Inglis BA. Considerations of marrow cellularity in 3-dimensional dosimetric models of the trabecular skeleton. *J Nucl Med.* 2002;43(1):97-108.
- (145) Zanzonico PB. Model-based versus patient-specific dosimetry: blurring the lines. *J Nucl Med.* 2002;43(12):1665-1666.

Populärvetenskaplig sammanfattning

En del sjukdomstillstånd kan både undersökas och behandlas med hjälp av radioaktiva läkemedel som ges till patienten vanligtvis genom injektion. Vid undersökning ger dessa ämnen i allmänhet låga stråldoser till patienten. Vid cancerbehandling med radioaktiva läkemedel t.ex. radioaktivt märkta monoklonala antikroppar, är avsikten att tumörcellerna ska få en så hög stråldos att dessa dör, utan att den friska vävnaden skadas. För att kunna göra en noggrann beräkning av stråldosen till olika organ och celler, måste det radioaktiva ämnets upptag och försvinnande från de olika organen kunna mätas. För varje patient som behandlas ska stråldosen beräknas till olika organ.

Upptaget av det radioaktiva ämnet mäts oftast med en gammakamera som ger bilder av ämnets fördelning i kroppen. Mätningar göres i två motsatta projektioner, framifrån och bakifrån, där det geometriska medelvärdet beräknas. I dessa bilder av det radioaktiva ämnets fördelning i kroppens organ, fås problem bland annat med att strålningen sprids i kroppen och ger ett bidrag i bilden som inte representerar var det radioaktiva ämnet tagits upp.

Genom att använda ett människolikande datorfantom, kan data från laboratoriestudier användas för hur det radioaktiva ämnet fördelar sig i kroppen vid olika tidpunkter och med sannolikhetsbaserade beräkningar med Monte Carlo metoden, erhålles en bild så som gammakameran skulle ha mätt upptaget. I dessa bilder har olika korrektionsmetoder för strålningens spridning och dämpning undersökts och olika data för beräkning av stråldoser har jämförts.

Även en detaljerad modell för stråldosberäkning för de strålningskänsliga cryptcellerna i tunntarmens slemhinna har utvecklats och förfinats. Tidigare modeller har endast tagit hänsyn till stråldosen från radioaktiva ämnen i tunntarmsinnehållet, medan denna nya modell även tar hänsyn till upptag i tarmväggen samt bidraget till stråldosen från mer avlägsna tarmmslingor.

Det är nödvändigt med noggrannare bestämning av mängden av det radioaktiva ämnet utifrån gammakamerabilderna i kombination med att stråldosmodellerna utvecklas och blir mer realistiska och kan göras mer patientspecifika. Genom att utnyttja detaljerade data för upptag och utsöndring i kombination med noggranna patientmätningar kan dessa knytas samman i anatomiskt detaljerade stråldosmodeller vilket bör leda till en noggrannare patientdosimetri.